NASA/TP—2012–215976

First- and Second-Order Displacement Transfer Functions for Structural Shape Calculations Using Analytically Predicted Surface Strains

William L. Ko and Van Tran Fleischer

Dryden Flight Research Center, Edwards, California

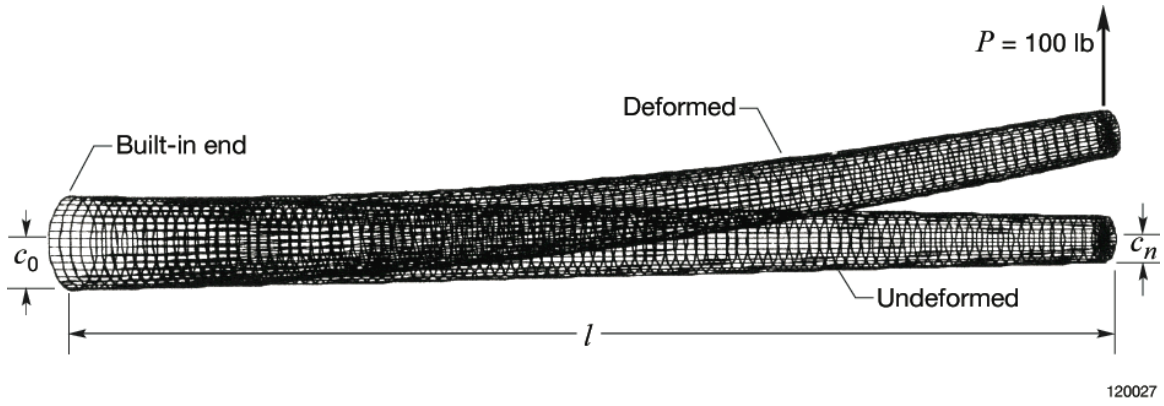

March 2012

NASA STI Program ... in Profile

Since its founding, NASA has been dedicated to the advancement of aeronautics and space science. The NASA scientific and technical information (STI) program plays a key part in helping NASA maintain this important role.

The NASA STI program operates under the auspices of the Agency Chief Information Officer. It collects, organizes, provides for archiving, and disseminates NASA's STI. The NASA STI program provides access to the NASA Aeronautics and Space Database and its public interface, the NASA Technical Report Server, thus providing one of the largest collections of aeronautical and space science STI in the world. Results are published in both non-NASA channels and by NASA in the NASA STI Report Series, which includes the following report types:

- TECHNICAL PUBLICATION. Reports of completed research or a major significant phase of research that present the results of NASA Programs and include extensive data or theoretical analysis. Includes compilations of significant scientific and technical data and information deemed to be of continuing reference value. NASA counterpart of peer-reviewed formal professional papers but has less stringent limitations on manuscript length and extent of graphic presentations.

- TECHNICAL MEMORANDUM. Scientific and technical findings that are preliminary or of specialized interest, e.g., quick release reports, working papers, and bibliographies that contain minimal annotation. Does not contain extensive analysis.

- CONTRACTOR REPORT. Scientific and technical findings by NASA-sponsored contractors and grantees.

- CONFERENCE PUBLICATION. Collected papers from scientific and technical conferences, symposia, seminars, or other meetings sponsored or co-sponsored by NASA.

- SPECIAL PUBLICATION. Scientific, technical, or historical information from NASA programs, projects, and missions, often concerned with subjects having substantial public interest.

- TECHNICAL TRANSLATION. English-language translations of foreign scientific and technical material pertinent to NASA's mission.

Specialized services also include organizing and publishing research results, distributing specialized research announcements and feeds, providing help desk and personal search support, and enabling data exchange services.

For more information about the NASA STI program, see the following:

- Access the NASA STI program home page at *http://www.sti.nasa.gov*

- E-mail your question via the Internet to help@sti.nasa.gov

- Fax your question to the NASA STI Help Desk at 443-757-5803

- Phone the NASA STI Help Desk at 443-757-5802

- Write to:
  NASA STI Help Desk
  NASA Center for AeroSpace Information
  7115 Standard Drive
  Hanover, MD 21076-1320

NASA/TP—2012–215976

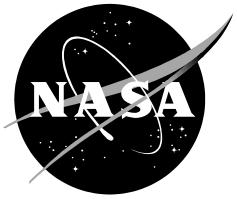

First- and Second-Order Displacement Transfer Functions for Structural Shape Calculations Using Analytically Predicted Surface Strains

William. L. Ko and Van Tran Fleischer

Dryden Flight Research Center, Edwards, California

National Aeronautics and
Space Administration

Dryden Flight Research Center
Edwards, CA 93523-0273

March 2012

The structural shape prediction method described in this report is protected under U.S. Patent No. 7,520,176, issued April 21, 2009. Therefore, those interested in using the method should contact the NASA Innovative Partnership Program Office at the Dryden Flight Research Center for more information.

Available from:

NASA Center for AeroSpace Information
7115 Standard Drive
Hanover, MD 21076-1320
443-757-5802

TABLE OF CONTENTS

ABSTRACT

New first- and second-order displacement transfer functions have been developed for deformed shape calculations of nonuniform cross-sectional beam structures such as aircraft wings. The displacement transfer functions are expressed explicitly in terms of beam geometrical parameters and surface strains (uniaxial bending strains) obtained at equally spaced strain stations along the surface of the beam structure. By inputting the measured or analytically calculated surface strains into the displacement transfer functions, one could calculate local slopes, deflections, and cross-sectional twist angles of the nonuniform beam structure for mapping the overall structural deformed shapes for visual display. The accuracy of deformed shape calculations by the first- and second-order displacement transfer functions are determined by comparing these values to the analytically predicted values obtained from finite-element analyses. This comparison shows that the new displacement transfer functions could quite accurately calculate the deformed shapes of tapered cantilever tubular beams with different tapered angles. The accuracy of the present displacement transfer functions also are compared to those of the previously developed displacement transfer functions.

NOMENCLATURE

c	depth factor (vertical distance from neutral axis to bottom surface of uniform beam), in.
c_i	depth factor (vertical distance from neutral axis to i-th strain station on bottom surface of nonuniform beam), in.
c_n	value of c_i at free end (beam tip), $x = x_n = l$, in.
c_n / c_0	beam depth ratio, dimensionless
$c(x)$	depth factor (vertical distance from neutral axis to bottom surface of nonuniform beam), in.
c_0	value of c_i at fixed end (beam root), $x = x_0 = 0$, in.
deg	degree
E	Young's modulus, lb/in^2
i	$= 0,\ 1,\ 2,\ 3,\ ...,\ n$, strain station identification number
I	moment of inertia, in^4
j	index
l	length of beam, in.
$M_i \equiv M(x_i)$, bending moment at strain station, x_i, in-lb	
$M(x)$	bending moment at axial location of beam, x, in-lb
n	index for last span-wise strain station (or domain density)
P	force, lb
SPAR	Stuctural Performance And Resizing
t	wall thickness of tubular beam, in.
x, y	Cartesian coordinates (x in axial direction of beam, y in vertical direction), in.
x_i	axial coordinate associated with i-th surface strain station, in.
y_i	$\equiv y(x_i)$, beam deflection in y-direction at axial location, $x = x_i$, in.
$y(x)$	beam deflection in y-direction at axial location, x, in.
α	$\equiv \tan^{-1}[(c_0 - c_n)/l]$ taper angle of beam, deg
Δl	$\equiv (x_i - x_{i-1}) = l/n$, distance between two adjacent strain stations $\{x_{i-1}, x_i\}$, in.
ε_i	$\equiv \varepsilon(x_i)$, surface bending strain at strain station, x_i, in/in
$\varepsilon(x)$	surface bending strain (axial strain) at axial location, x, in/in

θ_i $\equiv \theta(x_i)$, slope of deformed beam at axial location, $x = x_i$, rad or deg

$\theta(x)$ slope of deformed beam at axial location, x, rad or deg

σ_i $\equiv E\varepsilon_i$, axial stress associated with surface bending strain, ε_i, lb/in^2

$\sigma(x)$ $\equiv E\varepsilon(x)$, axial stress associated with surface bending strain, $\varepsilon(x)$, lb/in^2

INTRODUCTION

Recently, several displacement transfer functions were formulated for structural deformed shape calculations using surface strains (refs. 1–4). In the formulations of the displacement transfer functions, the beam-like structure (such as an aircraft wing) was discretized evenly into multiple small domains of the same length. Through such discretization, linear-variation assumptions could be made for both beam depth and surface strain within each small domain. This approach enabled the integrations of the classical beam differential equation in closed forms to yield beam slopes and deflections for each small domain. By combining the slope and deflection equations, one can write the final forms of the deflection equations, called displacement transfer functions, in terms of beam geometrical parameters and surface strains evaluated at evenly distributed inboard strain stations (at domain junctures). Thus, the displacement transfer functions can be used to convert the surface strains into displacements (deflections and angular rotations) at multiple domain junctures so that one can map out overall deformed shapes of the beam structures for visual display. Thus, the displacement transfer functions, with an accompanying surface strain–sensing system, has created a revolutionary new structural shape–sensing technology (ref. 5, *Method for Real-Time Structure Shape-Sensing,* Ko-Richards, U.S. Patent No. 7,520,176) for in-flight deformed shape monitoring of flexible wings and tails. In addition, the wing shape monitored in real time could then be input to the aircraft control system for aeroelastic wing shape control. Similar to the structural deformed shape calculations, the distributed surface strains also can be used to predict the structural operational loads (ref. 6, *Process for Using Surface Strain Measurements to Obtain Operational Loads for Complex Structures*, Richards-Ko, U.S. Patent No. 7,715,994) for flight vehicle operational load monitoring.

When the structural shape–sensing technology is applied, using the conventional strain gage system for sensing the surface strains of flight vehicles is impractical because of excessive lead wire weight. The most attractive candidate for a flight vehicle surface strain–sensing system, an alternative to the conventional strain gage system, is the fiber-optic strain-sensing system, because the fiber optics are lightweight, fine, and flexible filaments (approximately the size of human hairs), and they can be highly multiplexed (Bragg gratings) to define the strain-sensing points at desired sensing intervals (refs. 7–9). Another powerful characteristic of the fiber-optic strain-sensing system is that, for sensing a given structure, the needed number of actual strain data extraction points can be easily specified by means of a single command.

The displacement transfer functions were originally developed for deformed shape predictions of straight beams and were successfully validated for accuracy by finite-element analyses of different sample structures, such as cantilever tubular beams (uniform, tapered, slightly tapered, stepwise tapered), two-point supported tapered tubular beams, flat panels, and tapered wing boxes (unswept and swept). The straight-beam displacement transfer functions were further extended to the shape predictions of slender curved structures by introducing curvature-effect collections (ref. 10).

In this report, the first- and second-order displacement transfer functions are developed for deformed shape predictions of nonuniform cantilever beam structures (such as aircraft wings). Analytically calculated surface strains are then input to the transfer functions, and structural shape calculations are made. The shape calculation accuracy of the newly formulated displacement transfer functions are then

compared with those of the earlier displacement transfer functions (ref. 2) developed for nonuniform and slightly nonuniform cantilever structures.

BASICS OF DISPLACEMENT TRANSFER FUNCTIONS

The basics of the displacement transfer functions previously formulated (refs. 1–4) for shape predictions of cantilever straight beams using distributed surface strains are briefly described in this section. The piecewise-linear assumptions made in the formulation of the displacement transfer functions also are discussed.

Beam Differential Equations

The formulation of the displacement transfer functions stems from the classical beam differential equation (elastic curvature of the deformed straight uniform beam) given by (refs. 11–12)

$$\frac{d^2y}{dx^2} = \frac{M(x)}{EI} \tag{1}$$

in which y is the vertical deflection, x is the beam axial coordinate, $M(x)$ is the bending moment, E is the Young's modulus, and I is the cross-sectional moment of inertia. Equation (1) can be applied to a nonuniform beam segment with sufficient accuracy if the beam cross sections change gradually (weak nonuniform beam) (ref. 11, p. 143). For the weak nonuniform beam case, I is a weak function of x, and over a short beam segment, the average value can be used.

At the cross-section, x, the bending moment, $M(x)$, and associated bending strain (axial strain), $\varepsilon(x)[=\sigma(x)/E]$, at the bottom surface point of the nonuniform straight beam can be written as

$$M(x) = I\frac{\sigma(x)}{c(x)} = EI\frac{\varepsilon(x)}{c(x)} \tag{2}$$

in which $c(x)$ is the beam depth factor (vertical distance from the neutral axis to the bottom surface of the nonuniform beam, or half depth if the neutral axis is located at the half depth of the beam). For a tubular beam case, $c(x)$ will be the outer radius. The sign convention of equation (2) is for the positive bending moment, $M(x)$ (bending the cantilever beam upward; fig. 1), to induce a positive bending strain, $\varepsilon(x)$, on the bottom surface of the beam. Combining equations (1) and (2), one obtains the modified differential equation for the nonuniform beam as

$$\frac{d^2y}{dx^2} = \frac{\varepsilon(x)}{c(x)} \tag{3}$$

Note that the modified beam differential equation (3) contains only the beam depth factor, $c(x)$, and the surface bending strain, $\varepsilon(x)$. The flexural rigidity, EI, is eliminated. The formulation of the displacement transfer functions for the nonuniform straight beam is based upon the modified beam differential equation (3), which could be sufficiently accurate if the nonuniform beam cross sections

change gradually (ref. 11, p. 143). If the mathematical functional forms of $\{c(x), \varepsilon(x)\}$ are known, equation (3) can be integrated once to yield the beam slope, $dy/dx[\equiv \tan\theta(x)]$, and then integrated a second time to yield the beam deflection, $y(x)$, for each small domain needed for the structural deformed shape predictions.

Discretization

To carry out the single and double integrations of equation (3) in closed forms, the nonuniform cantilever beam of length l was discretized into n number of small domains of equal length, $\Delta l(= l/n)$ (fig. 1). The i-th $(i = 0, 1, 2, 3, ..., n)$ strain stations are to be located on the bottom surface of the domain junctures, $x = x_i$ $(i = 0, 1, 2, 3, ..., n)$ (called strain stations, x_i). Note from figure 1 that the first and last strain stations $\{x_0, x_n\}$ are located at the fixed end $(x = x_0 = 0)$ and at the free end $(x = x_n = l)$, respectively. Within each small domain, $x_{i-1} \le x \le x_i$, between the two adjacent strain stations, $\{x_{i-1}, x_i\}$, the following piecewise linear assumptions can be made with sufficient accuracy for slowly changing functions.

Basic Assumptions

The following two basic assumptions are needed for deriving the displacement transfer functions:

1. Within the small domain, $x_{i-1} \le x \le x_i$, between the two adjacent strain stations, $\{x_{i-1}, x_i\}$, the depth factor, $c(x)$, can be represented with a linear function of $(x - x_{i-1})$, as

$$c(x) = c_{i-1} - (c_{i-1} - c_i)\frac{x - x_{i-1}}{\Delta l} \quad ; \quad x_{i-1} \le x \le x_i \tag{4}$$

   in which $\{c_{i-1}, c_i\}$ are the values of $c(x)$ at the strain stations, $\{x_{i-1}, x_i\}$, respectively.

2. Within the small domain, $x_{i-1} \le x \le x_i$, between the two adjacent strain stations, $\{x_{i-1}, x_i\}$, the bottom surface bending strain, $\varepsilon(x)$, also can be assumed to vary linearly with $(x - x_{i-1})$, as

$$\varepsilon(x) = \varepsilon_{i-1} - (\varepsilon_{i-1} - \varepsilon_i)\frac{x - x_{i-1}}{\Delta l} \quad ; \quad x_{i-1} \le x \le x_i \tag{5}$$

   in which $\{\varepsilon_{i-1}, \varepsilon_i\}$ are the values of $\varepsilon(x)$ at the strain stations, $\{x_{i-1}, x_i\}$, respectively.

If $\varepsilon(x)$ is a strong nonlinear function of x, the domain length, Δl, should be reduced so that the piecewise linear assumption of equation (5) can remain as a good approximation.

Linearity of Bending Moment

Substituting equations (4) and (5) into equation (2), and expanding the factor, $1/c(x)$, in binomial series form because of a small coefficient $(c_i - c_{i-1})$ of the slope term (weak nonuniform beam), one obtains

$$M(x) = EI\frac{\varepsilon(x)}{c(x)}$$

$$= EI\frac{\varepsilon_{i-1}}{c_{i-1}}\left[1-\left(1-\frac{\varepsilon_i}{\varepsilon_{i-1}}\right)\frac{x-x_{i-1}}{\Delta l}\right]\left[1+\left(1-\frac{c_i}{c_{i-1}}\right)\frac{x-x_{i-1}}{\Delta l}+\left(1-\frac{c_i}{c_{i-1}}\right)^2\frac{(x-x_{i-1})^2}{(\Delta l)^2}+....\right] \qquad (6)$$

For a weak nonuniform beam, $(1-c_i/c_{i-1})$ is small (that is, $(1-c_i/c_{i-1})<<1$), and within the small domain, $x_{i-1}\le x\le x_i$, if the average value of I is used, the bending moment, $M(x)$, within the domain, $x_{i-1}\le x\le x_i$, will vary almost linearly because higher order terms in $(1-c_i/c_{i-1})$ can be neglected. For a moderate nonuniform beam, however, the value of $(1-c_i/c_{i-1})$ is no longer very small, and the higher order terms must be retained. This retention of the higher order terms will cause $M(x)$ to be slightly nonlinear over the domain, $x_{i-1}\le x\le x_i$.

For the uniform beam ($c(x)=c=$ constant), the bending moment, $M(x)$, is directly proportional to the bending strain, $\varepsilon_i(x)$, according to equation (2). Therefore, if the bending moment, $M(x)$, is a linear function of x, then the bending strain, $\varepsilon(x)$, also will be a linear function of x.

Basic Slope Equations

The slope, $\tan\theta(x)(\equiv dy/dx)$, of the nonuniform beam at the axial location, x, within the domain, $x_{i-1}\le x\le x_i$ (fig. 1), can be obtained by integrating equation (3) once, and enforcing the continuity of the slope at the inboard strain station, x_{i-1}, as

$$\tan\theta(x) = \underbrace{\int_{x_{i-1}}^{x}\frac{d^2y}{dx^2}dx}_{\text{Integration of eq. (3)}} + \underbrace{\tan\theta_{i-1}}_{\text{Slope at } x_{i-1}} = \underbrace{\int_{x_{i-1}}^{x}\frac{\varepsilon(x)}{c(x)}dx}_{\substack{\text{Slope increment}\\ \text{above } \tan\theta_{i-1}}} + \underbrace{\tan\theta_{i-1}}_{\text{Slope at } x_{i-1}} \quad ;\ (x_{i-1}\le x\le x_i) \qquad (7)$$

in which $\tan\theta_{i-1}$ is the slope at the inboard strain station, x_{i-1}. In light of the piecewise linear assumptions of $\{c(x),\varepsilon(x)\}$ given by equations (4) and (5), respectively, equation (7) can be written in the form

$$\tan\theta(x) = \int_{x_{i-1}}^{x}\frac{\varepsilon_{i-1}-(\varepsilon_{i-1}-\varepsilon_i)\dfrac{x-x_{i-1}}{\Delta l}}{c_{i-1}-(c_{i-1}-c_i)\dfrac{x-x_{i-1}}{\Delta l}}dx+\tan\theta_{i-1} \quad ;\ (x_{i-1}\le x\le x_i) \qquad (8)$$

Note that the direct integration of equation (8) will result in a slope equation of the form (ref. 1, eq. (23))

$$\tan\theta_i = \Delta l\left[\frac{\varepsilon_{i-1}-\varepsilon_i}{c_{i-1}-c_i}+\frac{\varepsilon_{i-1}c_i-\varepsilon_i c_{i-1}}{(c_{i-1}-c_i)^2}\log_e\frac{c_i}{c_{i-1}}\right]+\tan\theta_{i-1}\quad;\quad (i=1,\ 2,\ 3,\ ...,\ n) \tag{9}$$

in which $\tan\theta_i[\equiv\tan\theta(x_i)]$ is the slope at the strain station, x_i. Note from equation (9) that in the limit, $c_i/c_{i-1}=1$, for the uniform beam, the first term, $(\varepsilon_{i-1}-\varepsilon_i)/(c_{i-1}-c_i)$, will go to infinity, and the second term with the factor, $\left[\log_e(c_i/c_{i-1})\right]/(c_{i-1}-c_i)^2$, will become mathematically indeterminate (that is, $0/0$). To circumvent this limit-case mathematical breakdown problem, the logarithmic term must be expanded in terms of a $(c_{i-1}-c_i)$ series in the vicinity of $c_i/c_{i-1}\approx 1$, so that the denominators containing the factor, $(c_{i-1}-c_i)$, can be cancelled out. After mathematical manipulations are carried out, equation (9) can be reduced to the form (ref. 1, eq. (27))

$$\tan\theta_i = \frac{\Delta l}{2c_{i-1}}\left[\left(2-\frac{c_i}{c_{i-1}}\right)\varepsilon_{i-1}+\varepsilon_i\right]+\tan\theta_{i-1}\quad;\quad (i=1,\ 2,\ 3,\ ...,\ n) \tag{10}$$

which is now applicable to the limit case, $c_i/c_{i-1}=1$, of the uniform beam.

Basic Deflection Equations

The deflection, $y(x)$, of the nonuniform beam within the domain, $x_{i-1}\le x\le x_i$ (fig. 1), can be obtained by integrating the slope equation (7) and enforcing the continuity of the deflection at the inboard adjacent strain station, x_{i-1}, as

$$y(x)=\underbrace{\int_{x_{i-1}}^{x}\tan\theta(x)\,dx}_{\text{Integration of slope}}+\underbrace{y_{i-1}}_{\substack{\text{Deflection}\\ \text{at } x_{i-1}}}=\underbrace{\int_{x_{i-1}}^{x}\int_{x_{i-1}}^{x}\frac{\varepsilon(x)}{c(x)}dx\,dx}_{\text{Deflection increment above } y_{i-1}}+\underbrace{\int_{x_{i-1}}^{x}\tan\theta_{i-1}dx}_{\substack{\text{Deflection at } x\\ \text{due to } \tan\theta_{i-1}}}+\underbrace{y_{i-1}}_{\substack{\text{Deflection}\\ \text{at } x_{i-1}}}$$

$$(x_{i-1}\le x\le x_i) \tag{11}$$

in which y_{i-1} is the deflection at the inboard strain station, x_{i-1}.

In light of the piecewise linear assumptions of $\{c(x),\varepsilon(x)\}$ given by equations (4) and (5), respectively, the deflection equation (11) takes on the form

$$y(x)=\int_{x_{i-1}}^{x}\int_{x_{i-1}}^{x}\frac{1-\left(1-\dfrac{\varepsilon_i}{\varepsilon_{i-1}}\right)\dfrac{x-x_{i-1}}{\Delta l}}{1-\left(1-\dfrac{c_i}{c_{i-1}}\right)\dfrac{x-x_{i-1}}{\Delta l}}dx\,dx+\int_{x_{i-1}}^{x}\tan\theta_{i-1}\,dx+y_{i-1}\quad;\quad (x_{i-1}\le x\le x_i) \tag{12}$$

Note that direct integration of equation (12) will yield the deflection equation in the form (ref. 1, eq. (25))

$$y_i = (\Delta l)^2 \left\{ \frac{\varepsilon_{i-1} - \varepsilon_i}{2(c_{i-1} - c_i)} - \frac{\varepsilon_{i-1} c_i - \varepsilon_i c_{i-1}}{(c_{i-1} - c_i)^3} \left[c_i \log_e \frac{c_i}{c_{i-1}} + (c_{i-1} - c_i) \right] \right\} + y_{i-1} + \Delta l \tan\theta_{i-1}$$

$$(i = 1,\ 2,\ 3,\ldots,\ n) \qquad (13)$$

in which $y_i [\equiv y(x_i)]$ is the deflection at the strain station, x_i. Note from equation (13) that in the limit, $c_i / c_{i-1} = 1$, for a uniform beam case, the first and third terms with the factor, $(c_{i-1} - c_i)$, in the denominators will go to infinity, and the second term with the factor, $\left[\log_e (c_i / c_{i-1})\right] / (c_{i-1} - c_i)^3$, will become mathematically indeterminate (that is, $0/0$). To circumvent this limit-case mathematical breakdown problem, the logarithmic term must be expanded in terms of a $(c_{i-1} - c_i)$ series in the neighborhood of $c_i / c_{i-1} \approx 1$ so that the denominators containing the factor, $(c_{i-1} - c_i)$, can be cancelled out. After the mathematical manipulations are carried out, equation (13) can be reduced to the form (ref. 1, eq. (30))

$$y_i = \frac{(\Delta l)^2}{6 c_{i-1}} \left[\left(3 - \frac{c_i}{c_{i-1}} \right) \varepsilon_{i-1} + \varepsilon_i \right] + y_{i-1} + \Delta l \tan\theta_{i-1} \quad ;\ (i = 1,\ 2,\ 3,\ \ldots,\ n) \qquad (14)$$

which is now applicable to the limit case, $c_i / c_{i-1} = 1$, of the uniform beam.

ALTERNATIVE DISPLACEMENT TRANSFER FUNCTIONS

To circumvent the aforementioned limit-case mathematical problems, the development of alternative displacement transfer functions for the nonuniform cantilever beam is needed. The new alternative displacement transfer functions also must be applicable to the limit case of a uniform beam without creating limit-case mathematical indeterminacy problems. Because the cantilever beam is assumed to be a weak nonuniform beam (that is, $1 - (c_i / c_{i-1}) << 1$), the perturbation method can be applied to formulate the new displacement transfer functions by expanding the factor, $1 / c(x)$, in the integrand of equations (8) or (12) in binomial series form up to the first- or second-order terms. The formulations of the new first- and second-order displacement transfer functions are presented in the following sections. Appendices A and B present the detailed mathematical derivations for readers to easily follow.

FIRST-ORDER DISPLACEMENT TRANSFER FUNCTION

In this section, the first-order slope equations and first-order deflection equations are formulated for the nonuniform cantilever beam. Appendix A presents the detailed mathematical derivations.

First-Order Slope Equations

Under the assumption of the present weak nonuniform cantilever beam for which $(1-c_i/c_{i-1}) \ll 1$, the factor, $\left[1-\left(1-\frac{c_i}{c_{i-1}}\right)\frac{x-x_{i-1}}{\Delta l}\right]^{-1}$, in the integrand of the slope equation (8) can be expanded in binomial series form up to the first-order term to yield

$$\tan\theta(x) = \frac{\varepsilon_{i-1}}{c_{i-1}}\int_{x_{i-1}}^{x_i}\left[1-\left(1-\frac{\varepsilon_i}{\varepsilon_{i-1}}\right)\frac{x-x_{i-1}}{\Delta l}\right]\left[1+\left(1-\frac{c_i}{c_{i-1}}\right)\frac{x-x_{i-1}}{\Delta l}+\ldots\right]dx + \tan\theta_{i-1}$$

$$(x_{i-1} \le x \le x_i) \qquad (15)$$

in which $\tan\theta_{i-1}$ $[\equiv \tan\theta(x_{i-1})]$ is the slope at $x = x_{i-1}$.

After carrying out the integration of equation (15) (ref. 13), one obtains the first-order slope equation for the domain, $x_{i-1} \le x \le x_i$ (see Appendix A for detailed derivations),

$$\tan\theta(x) = \frac{\varepsilon_{i-1}}{c_{i-1}}\left[(x-x_{i-1}) + \left(\frac{\varepsilon_i}{\varepsilon_{i-1}}-\frac{c_i}{c_{i-1}}\right)\frac{(x-x_{i-1})^2}{2\Delta l} - \left(1-\frac{\varepsilon_i}{\varepsilon_{i-1}}\right)\left(1-\frac{c_i}{c_{i-1}}\right)\frac{(x-x_{i-1})^3}{3(\Delta l)^2}\right] + \tan\theta_{i-1}$$

$$(x_{i-1} \le x \le x_i) \qquad (16)$$

At the strain station, x_i, we have $(x_i - x_{i-1}) = \Delta l$, and equation (16) takes on the form (see Appendix A)

$$\tan\theta_i = \frac{\Delta l}{6c_{i-1}}\left[\left(4-\frac{c_i}{c_{i-1}}\right)\varepsilon_{i-1} + \left(5-2\frac{c_i}{c_{i-1}}\right)\varepsilon_i\right] + \tan\theta_{i-1} \quad ; \ (i = 1,\ 2,\ 3,\ \ldots,\ n) \qquad (17)$$

in which $\tan\theta_i$ $[\equiv \tan\theta(x_i)]$ is the slope at $x = x_i$. Equation (17) is the first-order slope equation in a descending recursion relationship. Applying the descending recursion relationships, one can rewrite equation (17) in a series summation form for the strain station, x_i, as

$$\tan\theta_i = \frac{\Delta l}{6}\sum_{j=1}^{i}\frac{1}{c_{j-1}}\left[\left(4-\frac{c_j}{c_{j-1}}\right)\varepsilon_{j-1} + \left(5-2\frac{c_j}{c_{j-1}}\right)\varepsilon_j\right] + \underbrace{\tan\theta_0}_{=0 \text{ for cantilever beams}} \quad ; \ (i = 1,\ 2,\ 3,\ \ldots,\ n) \qquad (18)$$

Equation (18) is the final form of the first-order slope equation in series summation form for the nonuniform cantilever beam.

For the uniform beam case ($c_i = c_{i-1} = c$), equation (18) degenerates into the form

$$\tan\theta_i = \frac{\Delta l}{2c}\sum_{j=1}^{i}(\varepsilon_{j-1}+\varepsilon_j) + \underbrace{\tan\theta_0}_{=0 \text{ for cantilever beams}} \quad ; \quad (i = 1,\ 2,\ 3,\ ...,\ n) \tag{19}$$

which agrees with previously established equation (25) of reference 2.

First-Order Deflection Equations

The deflection, $y(x)$, of the nonuniform cantilever beam within the domain, $x_{i-1} \le x \le x_i$, can be obtained by integrating the slope equation (16) (ref. 13), and enforcing the continuity of the deflection at the inboard adjacent strain station, x_{i-1}, as (see Appendix A)

$$\begin{aligned} y(x) &= \int_{x_{i-1}}^{x} \underbrace{\tan\theta(x)}_{\text{eq. (16)}} dx + y_{i-1} \\ &= \frac{(x-x_{i-1})^2}{12}\frac{\varepsilon_{i-1}}{c_{i-1}}\left\{6 + 2\left(\frac{\varepsilon_i}{\varepsilon_{i-1}} - \frac{c_i}{c_{i-1}}\right)\frac{(x-x_{i-1})}{\Delta l} - \left(1-\frac{\varepsilon_i}{\varepsilon_{i-1}}\right)\left(1-\frac{c_i}{c_{i-1}}\right)\frac{(x-x_{i-1})^2}{(\Delta l)^2}\right\} \\ &\qquad + (x-x_{i-1})\tan\theta_{i-1} + y_{i-1} \\ &\qquad\qquad (x_{i-1} \le x \le x_i) \end{aligned} \tag{20}$$

in which y_{i-1} is the deflection at the inboard strain station, x_{i-1}.

At the strain station, x_i, we have $(x_i - x_{i-1}) = \Delta l$, and equation (20) yields the deflection in the form (see Appendix A)

$$y_i = \frac{(\Delta l)^2}{12c_{i-1}}\left[\left(5-\frac{c_i}{c_{i-1}}\right)\varepsilon_{i-1} + \left(3-\frac{c_i}{c_{i-1}}\right)\varepsilon_i\right] + y_{i-1} + \Delta l\tan\theta_{i-1} \quad ; \quad (i = 1,\ 2,\ 3,\ ...,\ n) \tag{21}$$

in which $y_i[\equiv y(x_i)]$ is the deflection at the strain station, x_i. Equation (21) is the first-order deflection equation in a descending recursion relationship.

For a uniform beam ($c_i = c_{i-1} = c$), equation (21) degenerates into the form

$$y_i = \frac{(\Delta l)^2}{6c}\left(2\varepsilon_{i-1} + \varepsilon_i\right) + y_{i-1} + \Delta l \tan\theta_{i-1} \quad ; \ (i = 1,\ 2,\ 3,\ ...,\ n) \tag{22}$$

which agrees with the previously established equation (26) of reference 2.

Substituting the slope equation (18) into the deflection equation (21), with descending recursion relationships applied, yields (see Appendix A for derivations)

$$y_i = \frac{(\Delta l)^2}{12}\sum_{j=1}^{i}\frac{1}{c_{i-j}}\left\{\left[5 + 8(j-1) - \langle 1 + 2(j-1)\rangle\frac{c_{i-j+1}}{c_{i-j}}\right]\varepsilon_{i-j} + \left[3 + 10(j-1) - \langle 1 + 4(j-1)\rangle\frac{c_{i-j+1}}{c_{i-j}}\right]\varepsilon_{i-j+1}\right\} + \underbrace{y_0 + (i)\Delta l \tan\theta_0}_{=0 \text{ for cantilever beams}}$$
$$(i = 1,\ 2,\ 3,\ ...,\ n) \tag{23}$$

Equation (23) is the final form of the first-order deflection equation in series summation form (called the first-order displacement transfer function) for the nonuniform cantilever beam.

For the uniform beam case ($c_i = c_{i-1} = c$), equation (23) degenerates into

$$y_i = \frac{(\Delta l)^2}{6c}\sum_{j=1}^{i}\left[(3j-1)\varepsilon_{i-j} + (3j-2)\varepsilon_{i-j+1}\right] + \underbrace{y_0 + (i)\Delta l \tan\theta_0}_{=0 \text{ for cantilever beams}} \quad ; \ (i = 1,\ 2,\ 3,\ ...,\ n) \tag{24}$$

which is identical to equation (27) of reference 2.

After the terms are grouped, equation (24) can be rewritten in the alternative form (see Appendix A for derivations)

$$y_i = \frac{(\Delta l)^2}{6c}\left[(3i-1)\varepsilon_0 + 6\sum_{j=1}^{i-1}(i-j)\varepsilon_j + \varepsilon_i\right] + \underbrace{y_0 + (i)\Delta l \tan\theta_0}_{=0 \text{ for cantilever beams}} \quad ; \ (i = 1,\ 2,\ 3,\ ...,\ n) \tag{25}$$

which agrees with equation (28) of reference 2.

SECOND-ORDER DISPLACEMENT TRANSFER FUNCTION

In this section, the second-order slope equations and second-order deflection equations are formulated for the nonuniform cantilever beam. Appendix B presents the detailed mathematical derivations.

Second-Order Slope Equations

For the weak nonuniform beam with a slowly changing depth (that is, $(1-c_i/c_{i-1}) << 1$), accuracy of the displacement transfer functions can be improved by expanding the factor, $\left[1-\left(1-\frac{c_i}{c_{i-1}}\right)\frac{x-x_{i-1}}{\Delta l}\right]^{-1}$, in the integrand of the slope equation (8) in binomial series form up to the second-order term as

$$\tan\theta(x) = \frac{\varepsilon_{i-1}}{c_{i-1}}\int_{x_{i-1}}^{x}\left[1-\left(1-\frac{\varepsilon_i}{\varepsilon_{i-1}}\right)\frac{x-x_{i-1}}{\Delta l}\right]\left[1+\left(1-\frac{c_i}{c_{i-1}}\right)\frac{x-x_{i-1}}{\Delta l}+\left(1-\frac{c_i}{c_{i-1}}\right)^2\frac{(x-x_{i-1})^2}{(\Delta l)^2}+....\right]dx + \tan\theta_{i-1}$$

$$(x_{i-1} \le x \le x_i) \quad (26)$$

in which $\tan\theta_{i-1}$ is the slope at the inboard strain station, x_{i-1}.

After carrying out the integration of equation (26), one obtains the second-order slope equation for the domain, $x_{i-1} \le x \le x_i$, as (see Appendix B for details)

$$\tan\theta(x) = \frac{\varepsilon_{i-1}}{c_{i-1}}\left\{(x-x_{i-1})+\left(\frac{\varepsilon_i}{\varepsilon_{i-1}}-\frac{c_i}{c_{i-1}}\right)\frac{(x-x_{i-1})^2}{2\Delta l}+\left(1-\frac{c_i}{c_{i-1}}\right)\left(\frac{\varepsilon_i}{\varepsilon_{i-1}}-\frac{c_i}{c_{i-1}}\right)\frac{(x-x_{i-1})^3}{3(\Delta l)^2}\right.$$
$$\left.-\left(1-\frac{c_i}{c_{i-1}}\right)^2\left(1-\frac{\varepsilon_i}{\varepsilon_{i-1}}\right)\frac{(x-x_{i-1})^4}{4(\Delta l)^3}\right\}+\tan\theta_{i-1}$$

$$(x_{i-1} \le x \le x_i) \quad (27)$$

At the strain station, $x = x_i$, we have $(x_i - x_{i-1}) = \Delta l$, and equation (27) becomes (see Appendix B)

$$\tan\theta_i = \frac{\Delta l}{12c_{i-1}}\left\{\left[9-4\frac{c_i}{c_{i-1}}+\left(\frac{c_i}{c_{i-1}}\right)^2\right]\varepsilon_{i-1}+\left[13-10\frac{c_i}{c_{i-1}}+3\left(\frac{c_i}{c_{i-1}}\right)^2\right]\varepsilon_i\right\}+\tan\theta_{i-1}$$

$$(i = 1,\ 2,\ 3,\ ...,\ n) \quad (28)$$

in which $\tan\theta_i [\equiv \tan\theta(x_i)]$ is the slope at the strain station, x_i. Equation (28) is the second-order slope equation in a descending recursion relationship. Applying the descending recursion relationships, one can write equation (28) in series summation form as

$$\tan\theta_i = \frac{\Delta l}{12}\sum_{j=1}^{i}\frac{1}{c_{j-1}}\left\{\left[9-4\frac{c_j}{c_{j-1}}+\left(\frac{c_j}{c_{j-1}}\right)^2\right]\varepsilon_{j-1}+\left[13-10\frac{c_j}{c_{j-1}}+3\left(\frac{c_j}{c_{j-1}}\right)^2\right]\varepsilon_j\right\}+\underbrace{\tan\theta_0}_{=0 \text{ for cantilever beams}}$$

$$(i=1,\ 2,\ 3,\ ...,\ n) \qquad (29)$$

Equation (29) is the final form of the second-order slope equation in series summation form for the nonuniform cantilever beam.

For the uniform beam case ($c_i = c_{i-1} = c$), the second-order slope equation (29) degenerates into

$$\tan\theta_i = \frac{\Delta l}{2c}\sum_{j=1}^{i}(\varepsilon_{j-1}+\varepsilon_j)+\underbrace{\tan\theta_0}_{=0 \text{ for cantilever beams}} \quad ;\ (i=1,\ 2,\ 3,\ ...,\ n) \qquad (30)$$

which agrees with equation (25) of reference 2.

Second-Order Deflection Equations

The deflection, $y(x)$, of the nonuniform beam within the domain, $x_{i-1} \le x \le x_i$, can be obtained by integrating the slope equation (27), and enforcing the continuity of the deflection at the inboard adjacent strain station, x_{i-1}, as

$$\begin{aligned} y(x) &= \int_{x_{i-1}}^{x}\underbrace{\tan\theta(x)}_{\text{eq. (27)}}dx + y_{i-1} \\ &= \frac{\varepsilon_{i-1}}{2c_{i-1}}\left\{(x-x_{i-1})^2+\frac{1}{3}\left(\frac{\varepsilon_i}{\varepsilon_{i-1}}-\frac{c_i}{c_{i-1}}\right)\frac{(x-x_{i-1})^3}{\Delta l}+\frac{1}{6}\left(1-\frac{c_i}{c_{i-1}}\right)\left(\frac{\varepsilon_i}{\varepsilon_{i-1}}-\frac{c_i}{c_{i-1}}\right)\frac{(x-x_{i-1})^4}{(\Delta l)^2}\right. \\ &\qquad \left.-\frac{1}{10}\left(1-\frac{c_i}{c_{i-1}}\right)^2\left(1-\frac{\varepsilon_i}{\varepsilon_{i-1}}\right)\frac{(x-x_{i-1})^5}{(\Delta l)^3}\right\}+y_{i-1}+(x-x_{i-1})\tan\theta_{i-1} \end{aligned}$$

$$(x_{i-1} \le x \le x_i) \qquad (31)$$

in which y_{i-1} is the deflection at the inboard strain station, x_{i-1}.

At the strain station, x_i, we have $(x_i - x_{i-1}) = \Delta l$, and equation (31) becomes (see Appendix B)

$$y_i = \frac{(\Delta l)^2}{60 c_{i-1}} \left\{ \left[27 - 9\frac{c_i}{c_{i-1}} + 2\left(\frac{c_i}{c_{i-1}}\right)^2 \right] \varepsilon_{i-1} + \left[18 - 11\frac{c_i}{c_{i-1}} + 3\left(\frac{c_i}{c_{i-1}}\right)^2 \right] \varepsilon_i \right\} + y_{i-1} + \Delta l \tan\theta_{i-1}$$

$$(i = 1,\ 2,\ 3,\ ...,\ n) \qquad (32)$$

which is the second-order deflection equation in a descending recursion relationship.

For the uniform beam case ($c_i = c_{i-1} = c$), equation (32) degenerates into

$$y_i = \frac{(\Delta l)^2}{6c}(2\varepsilon_{i-1} + \varepsilon_i) + y_{i-1} + \Delta l \tan\theta_{i-1} \quad ; \quad (i = 1,\ 2,\ 3,\ ...,\ n) \qquad (33)$$

which is identical to equation (26) of reference 2.

Substituting the slope equation (29) into the deflection equation (32), with descending recursion relationships applied, yields (see Appendix B)

$$y_i = \frac{(\Delta l)^2}{60} \sum_{j=1}^{i} \frac{1}{c_{i-j}} \left\{ \left[27 + 45(j-1) - \langle 9 + 20(j-1) \rangle \frac{c_{i-j+1}}{c_{i-j}} + \langle 2 + 5(j-1) \rangle \left(\frac{c_{i-j+1}}{c_{i-j}}\right)^2 \right] \varepsilon_{i-j} \right.$$
$$\left. + \left[18 + 65(j-1) - \langle 11 + 50(j-1) \rangle \frac{c_{i-j+1}}{c_{i-j}} + \langle 3 + 15(j-1) \rangle \left(\frac{c_{i-j+1}}{c_{i-j}}\right)^2 \right] \varepsilon_{i-j+1} \right\} + \underbrace{y_0 + (i)\Delta l \tan\theta_0}_{=0 \text{ for cantilever beams}}$$

$$(i = 1,\ 2,\ 3,\ ...,\ n) \qquad (34)$$

Equation (34) is the final form of the second-order deflection equation in series summation form (called the second-order displacement transfer function) for the nonuniform cantilever beam.

For the uniform beam case ($c_i = c_{i-1} = c$), equation (34) degenerates into

$$y_i = \frac{(\Delta l)^2}{6c} \sum_{j=1}^{i} \left[(3j-1)\varepsilon_{i-j} + (3j-2)\varepsilon_{i-j+1} \right] + \underbrace{y_0 + (i)\Delta l \tan\theta_0}_{=0 \text{ for cantilever beams}} \quad ; \quad (i = 1,\ 2,\ 3,\ ...,\ n) \qquad (35)$$

which is identical to equation (27) of reference 2.

SUMMARY OF ALL DISPLACEMENT TRANSFER FUNCTIONS

This section summarizes all the displacement transfer functions previously developed (refs. 1, 2, 4). These transfer functions are listed for comparison of mathematical functional forms.

Previous Displacement Transfer Functions

The displacement transfer functions previously developed for nonuniform and slightly nonuniform straight cantilever beams have the following mathematical forms (refs. 1, 2, 4):

1. The displacement transfer function for the nonuniform cantilever straight beam ($c_i \neq c_{i-1}$) (derivations in ref. 2, Appendix A) is expressed as

$$y_i = (\Delta l)^2 \sum_{j=1}^{i} \left\{ [2(i-j)+1] \frac{\varepsilon_{j-1} - \varepsilon_j}{2(c_{j-1} - c_j)} - \frac{\varepsilon_{j-1} c_j - \varepsilon_j c_{j-1}}{(c_{j-1} - c_j)^3} \left[c_j \log \frac{c_j}{c_{j-1}} + (c_{j-1} - c_j) \right] \right\}$$
$$+ (\Delta l)^2 \sum_{j=1}^{i-1} (i-j) \left[\frac{\varepsilon_{j-1} c_j - \varepsilon_j c_{j-1}}{(c_{j-1} - c_j)^2} \log \frac{c_j}{c_{j-1}} \right] + \underbrace{y_0 + (i)\Delta l \tan\theta_0}_{=0 \text{ for cantilever beams}}$$
$$(i = 1,\ 2,\ 3,\ ...,\ n) \qquad (36)$$

Equation (36) is not applicable to the uniform beam because of mathematical indeterminacy problems at $c_i = c_{i-1} = c$.

2. The displacement transfer function for the slightly nonuniform cantilever straight beam ($c_i / c_{i-1} \to 1$) is expressed as

$$y_i = \frac{(\Delta l)^2}{6} \sum_{j=1}^{i} \frac{1}{c_{i-j}} \left\{ \left[3(2j-1) - (3j-2) \frac{c_{i-j+1}}{c_{i-j}} \right] \varepsilon_{i-j} + (3j-2) \varepsilon_{i-j+1} \right\} + \underbrace{y_0 + (i)\Delta l \tan\theta_0}_{=0 \text{ for cantilever beams}}$$
$$(i = 1,\ 2,\ 3,\ ...,\ n) \qquad (37)$$

which was obtained from equation (36) by expanding the logarithmic terms in series form in the neighborhood of $c_i / c_{i-1} \approx 1$ (derivations in ref. 2, Appendix C).

New Displacement Transfer Functions

The two new displacement transfer functions (23) and (34) developed in this report are duplicated as equations (38) and (39), respectively, as follows:

1. The first-order displacement transfer function (eq. (23)) is expressed as

$$y_i = \frac{(\Delta l)^2}{12} \sum_{j=1}^{i} \frac{1}{c_{i-j}} \left\{ \left[5 + 8(j-1) - \langle 1 + 2(j-1) \rangle \frac{c_{i-j+1}}{c_{i-j}} \right] \varepsilon_{i-j} \right.$$
$$\left. + \left[3 + 10(j-1) - \langle 1 + 4(j-1) \rangle \frac{c_{i-j+1}}{c_{i-j}} \right] \varepsilon_{i-j+1} \right\} + \underbrace{y_0 + (i)\Delta l \tan\theta_0}_{=0 \text{ for cantilever beams}}$$
$$(i = 1,\ 2,\ 3,\ ...,\ n) \qquad (38)$$

2. The second-order displacement transfer function (eq. (34)) is expressed as

$$y_i = \frac{(\Delta l)^2}{60}\sum_{j=1}^{i}\frac{1}{c_{i-j}}\left\{\left[27+45(j-1)-\left\langle 9+20(j-1)\right\rangle\frac{c_{i-j+1}}{c_{i-j}}+\left\langle 2+5(j-1)\right\rangle\left(\frac{c_{i-j+1}}{c_{i-j}}\right)^2\right]\varepsilon_{i-j}\right.$$
$$\left.+\left[18+65(j-1)-\left\langle 11+50(j-1)\right\rangle\frac{c_{i-j+1}}{c_{i-j}}+\left\langle 3+15(j-1)\right\rangle\left(\frac{c_{i-j+1}}{c_{i-j}}\right)^2\right]\varepsilon_{i-j+1}\right\}+\underbrace{y_0+(i)\Delta l\tan\theta_0}_{=0 \text{ for cantilever beams}}$$
$$(i=1,\ 2,\ 3,\ ...,\ n) \qquad (39)$$

3. The displacement transfer function for the uniform straight cantilever beam ($c_i = c_{i-1} = c$) (eq. (25)) is expressed as

$$y_i = \frac{(\Delta l)^2}{6c}\left[(3i-1)\varepsilon_0+6\sum_{j=1}^{i-1}(i-j)\varepsilon_j+\varepsilon_i\right]+\underbrace{y_0+(i)\Delta l\tan\theta_0}_{=0 \text{ for cantilever beams}} \quad ;\ (i=1,\ 2,\ 3,\ ...,\ n) \qquad (40)$$

Equation (40) is the degenerated form of equations (37), (38), and (39) for the uniform beam case ($c_i = c_{i-1} = c$) (see Appendices A and B).

Characteristics of Displacement Transfer Functions

Except for equation (36), equations (37), (38), and (39) could degenerate into equation (40) for the uniform beam case ($c_i = c_{i-1} = c$) without a mathematical indeterminacy problem (see Appendix A and Appendix B). Note that in each of the displacement transfer functions (36)–(40), the deflection, y_i, at the current strain station, x_i, is expressed in terms of domain length, Δl, inboard beam half depths ($c_0, c_1, c_2, c_3, \ldots, c_i$), and the associated inboard strains ($\varepsilon_0, \varepsilon_1, \varepsilon_2, \varepsilon_3, \ldots, \varepsilon_i$), including the values of c_i and ε_i at the current strain station, x_i, where the deflection, y_i, is calculated. Because deflection equations (36)–(40) contain no structural properties, in the deformed shape predictions of complex structures (such as aircraft wings), one can avoid tedious computations of bending stiffness, EI, at different strain stations (cross sections). In fact, the effect of EI is absorbed implicitly by the surface bending strains, ε_i. Thus, not needing to know EI is the powerful characteristic of the displacement transfer functions for structural deformed shape predictions.

ANALYTICAL SHAPE PREDICTIONS

The shape calculations in this report are referred to as an analytical shape prediction study. Namely, instead of using actual measured surface bending strains (which require actual flights or time-consuming ground tests), the Structural Performance And Resizing (SPAR) finite-element computer program (ref. 14) was used to generate the surface bending strains and beam deflections. The SPAR-generated deflection curves (assumed to be the correct deflection curves) were then used as reference points to check the accuracy of the corresponding deflection curves calculated from different displacement transfer functions.

The surface bending strains, ε_i ($i = 0, 1, 2, 3, ..., n$), at the i-th strain stations needed for inputs to calculate the beam deflections were generated by converting the SPAR-generated axial nodal stresses, σ_i ($i = 0, 1, 2, 3, ..., n$), at the i-th strain station into the associated bending strains, ε_i, through Hooke's law (that is, $\varepsilon_i = \sigma_i / E$), because the lateral stresses are practically zero for beam structures. Alternatively, the surface bending strains, ε_i, also can be generated from the axial length changes of the SPAR elements where the bending strains, ε_i, are to be obtained. This method was found to lose accuracy, however, near the highly bent beam tip region and therefore was not used. For accuracy verification, the SPAR-generated bending strains were then input to different displacement transfer functions for calculations of theoretical deflection curves for comparison with the corresponding SPAR-generated deflection curves.

COMPARISON OF SHAPE PREDICTION ACCURACY

In the following section, the shape prediction accuracy of the first- and second-order displacement transfer functions are compared with those of previous displacement functions developed for nonuniform and slightly nonuniform cantilever beams. For the comparative shape prediction accuracy studies, tapered cantilever tubular beams with different taper angles were chosen.

Tapered Cantilever Tubular Beams

For the tapered cantilever tubular beam (fig.1), the equally spaced strain stations will be along the bottom generatrix of the beam. Each of the tapered cantilever tubular beams analyzed has a radius that linearly decreases from the fixed end toward the free end. Table 1 lists the dimensions and taper angles, α, of the aluminum tapered tubular beams considered.

Table 1. Dimensions of aluminum tapered cantilever tubular beams.

l, in. (length)	t, in. (wall thickness)	c_0, in. (root depth)	c_n, in. (tip depth)	c_n / c_0 (depth ratio)	α {$= \tan^{-1}[(c_0 - c_n)/l]$}, deg (taper angle)
100.5	0.02296	4	4 (uniform)	4/4 (1.0)	0.00
100.5	0.02296	4	3	3/4 (0.75)	0.57
100.5	0.02296	4	2	2/4 (0.5)	1.14
100.5	0.02296	4	1	1/4 (0.25)	1.71
100.5	0.02296	4	0.5	0.5/4 (0.125)	1.99
100.5	0.02296	4	0.25	0.25/4 (0.0625)	2.14

Figure 2 shows the finite-element model of a typical tapered cantilever tubular beam (depth ratio of $c_n / c_0 = 2/4$) generated from the SPAR finite-element computer program (ref. 14). The size of the SPAR model (identical for all tapered beam cases) also is indicated in figure 2. The tapered cantilever tubular beam is subjected to an upward load of $P = 100$ lb at the beam tip. Figure 3 shows the SPAR-generated deformed shapes of the tapered cantilever tubular beams with different taper angles. For the higher taper angles (figs. 3d–f), the tapering down region near each beam tip is highly bent, and therefore, high bending strains are induced in this region (see next section).

Surface Bending Strains

Figure 4 shows the SPAR-generated surface bending strain curves for different tapered cantilever tubular beams under bending, using the domain density, n = 8 (the total number of strain stations is

$1+n=9$). The bending strain curve for the uniform beam case (c_n / c_0 = 4/4) is a classical straight line. For the tapered beams, however, the strain curves are bow shaped, and the bow bend becomes deeper as the depth ratio, c_n / c_0, decreases. At the depth ratio, c_n / c_0 = 0.5/4, the strain curve is deeply bent by nearly 130° toward the beam tip. When the depth ratio reaches the minimum of c_n / c_0 = 0.25/4, the strain curve changes to a "cat ear" shape with a nearly 160° sharp bend near the beam tip region where the strain reaches a maximum, and then sharply drops toward the beam tip. Note from figure 4 that the SPAR-generated strains are not exactly zero (theoretically zero) at the free beam tip (especially for the c_n / c_0 = 0.5/4 and c_n / c_0 = 0.25/4 cases) because of the discretization of the beam with finite elements (fig. 2).

Keep in mind that in the formulation of the present first- and second-order displacement transfer functions and all the previous displacement transfer functions, the distribution of the bending strain along the discretized cantilever beam was assumed to be piecewise linear (eq. (5)). Therefore, the strain curves used in the formulation should be piecewise-linear curves (connecting the two adjacent strain data points with straight lines) instead of the smooth strain curves shown in figure 4. For moderately bent strain curves (fig. 4), the piecewise-linear approximation could be quite accurate, but in a strongly bent region of the strain curve (that is, c_n / c_0 = 0.25/4, fig. 4), the piecewise linear approximation may lose some accuracy locally using the domain density of n = 8. Thus, for sharply bent strain curves, more strain data points (that is, increasing domain density, n) are needed to make the piecewise-linear strain curve approach the true smooth strain curves for improving the shape prediction accuracy (see the section entitled, "Domain Density").

Deflection Data

The strain data shown in figure 4 were input to deflection equations (36)–(40) for calculations of deflections of the tapered cantilever tubular beams with six depth ratios: c_n / c_0 = 4/4, 3/4, 2/4, 1/4, 0.5/4, 0.25/4. Tables 2a–f compare the resulting predicted deflections with the corresponding SPAR-generated deflections. The prediction errors produced by deflection equations (36)–(39) are indicated in parentheses for comparison. The percent prediction error at a strain station, x_i, produced by each deflection equation is defined as the difference between the predicted and SPAR-generated deflections divided by the associated SPAR-generated beam tip deflection.

Table 2a. Comparison of deflections calculated from SPAR with those calculated from different deflection equations; uniform cantilever tubular beam; c_n / c_0 = 4/4; n = 8.

Theories	y_0 (error, percent)	y_1 (error, percent)	y_2 (error, percent)	y_3 (error, percent)	y_4 (error, percent)	y_5 (error, percent)	y_6 (error, percent)	y_7 (error, percent)	y_8 (error, percent)
SPAR (reference)	0.00000 (0.0000)	0.01787 (0.0000)	0.06340 (0.0000)	0.13368 (0.0000)	0.22450 (0.0000)	0.33181 (0.0000)	0.45174 (0.0000)	0.57933 (0.0000)	0.71162 (0.0000)
Nonuniform, eq. (36)	--------	--------	--------	--------	--------	--------	--------	--------	--------
Slightly nonuniform, eq. (37)	0.00000 (0.0000)	0.01573 (0.3007)	0.06027 (0.4398)	0.12952 (0.5846)	0.21936 (0.7223)	0.32568 (0.8614)	0.44435 (1.0385)	0.57127 (1.1326)	0.70230 (1.3097)
First-order, eq. (38)	0.00000 (0.0000)	0.01573 (0.3007)	0.06027 (0.4398)	0.12952 (0.5846)	0.21936 (0.7223)	0.32568 (0.8614)	0.44435 (1.0385)	0.57127 (1.1326)	0.70230 (1.3097)
Second-order, eq. (39)	0.00000 (0.0000)	0.01573 (0.3007)	0.06027 (0.4398)	0.12952 (0.5846)	0.21936 (0.7223)	0.32568 (0.8614)	0.44435 (1.0385)	0.57127 (1.1326)	0.70230 (1.3097)

Table 2b. Comparison of deflections calculated from SPAR with those calculated from different deflection equations; tapered cantilever tubular beam; c_n / c_0 = 3/4; n = 8.

Theories	y_0 (error, percent)	y_1 (error, percent)	y_2 (error, percent)	y_3 (error, percent)	y_4 (error, percent)	y_5 (error, percent)	y_6 (error, percent)	y_7 (error, percent)	y_8 (error, percent)
SPAR (reference)	0.00000 (0.0000)	0.01823 (0.0000)	0.06697 (0.0000)	0.14572 (0.0000)	0.25204 (0.0000)	0.38294 (0.0000)	0.53428 (0.0000)	0.70092 (0.0000)	0.87634 (0.0000)
Nonuniform, eq. (36)	0.00000 (0.0000)	0.01623 (0.2282)	0.06407 (0.3309)	0.14180 (0.4473)	0.24707 (0.5671)	0.37676 (0.7052)	0.52686 (0.8467)	0.69210 (1.0065)	0.86568 (1.2164)
Slightly nonuniform, eq. (37)	0.00000 (0.0000)	0.01624 (0.2271)	0.06409 (0.3286)	0.14185 (0.4416)	0.24718 (0.5546)	0.37699 (0.6790)	0.52724 (0.8033)	0.69269 (0.9391)	0.86659 (1.1126)
First-order, eq. (38)	0.00000 (0.0000)	0.01623 (0.2282)	0.06405 (0.3332)	0.14175 (0.4530)	0.24699 (0.5763)	0.37665 (0.7178)	0.52669 (0.8661)	0.69187 (1.0327)	0.86538 (1.2507)
Second-order, eq. (39)	0.00000 (0.0000)	0.01623 (0.2282)	0.06407 (0.3309)	0.14179 (0.4485)	0.24706 (0.5683)	0.37676 (0.7052)	0.52686 (0.8467)	0.69209 (1.0076)	0.86567 (1.2176)

Table 2c. Comparison of deflections calculated from SPAR with those calculated from different deflection equations; tapered cantilever tubular beam; c_n / c_0 = 2/4; n = 8.

Theories	y_0 (error, percent)	y_1 (error, percent)	y_2 (error, percent)	y_3 (error, percent)	y_4 (error, percent)	y_5 (error, percent)	y_6 (error, percent)	y_7 (error, percent)	y_8 (error, percent)
SPAR (reference)	0.00000 (0.0000)	0.01864 (0.0000)	0.07113 (0.0000)	0.16057 (0.0000)	0.28831 (0.0000)	0.45510 (0.0000)	0.65965 (0.0000)	0.89759 (0.0000)	1.15801 (0.0000)
Nonuniform, eq. (36)	0.00000 (0.0000)	0.01681 (0.1580)	0.06855 (0.2228)	0.15709 (0.3005)	0.28385 (0.3851)	0.44936 (0.4957)	0.65236 (0.6295)	0.88815 (0.8152)	1.14592 (1.0440)
Slightly nonuniform, eq. (37)	0.00000 (0.0000)	0.01680 (0.1589)	0.06849 (0.2280)	0.15693 (0.3143)	0.28357 (0.4093)	0.44895 (0.5311)	0.65188 (0.6710)	0.88778 (0.8471)	1.14549 (1.0812)
First-order, eq. (38)	0.00000 (0.0000)	0.01679 (0.1598)	0.06848 (0.2288)	0.15690 (0.3169)	0.28348 (0.4171)	0.44873 (0.5510)	0.65137 (0.7150)	0.88672 (0.9387)	1.14334 (1.2668)
Second-order, eq. (39)	0.00000 (0.0000)	0.01681 (0.1580)	0.06855 (0.2228)	0.15708 (0.3014)	0.28383 (0.3869)	0.44932 (0.4991)	0.65230 (0.6347)	0.88807 (0.8221)	1.14518 (1.1079)

Table 2d. Comparison of deflections calculated from SPAR with those calculated from different deflection equations; tapered cantilever tubular beam; c_n / c_0 = 1/4; n = 8.

Theories	y_0 (error, percent)	y_1 (error, percent)	y_2 (error, percent)	y_3 (error, percent)	y_4 (error, percent)	y_5 (error, percent)	y_6 (error, percent)	y_7 (error, percent)	y_8 (error, percent)
SPAR (reference)	0.00000 (0.0000)	0.01912 (0.0000)	0.07598 (0.0000)	0.17923 (0.0000)	0.33816 (0.0000)	0.56506 (0.0000)	0.87454 (0.0000)	1.28196 (0.0000)	1.78417 (0.0000)
Nonuniform, eq. (36)	0.00000 (0.0000)	0.01742 (0.0953)	0.07372 (0.1267)	0.17627 (0.1659)	0.33448 (0.2063)	0.56030 (0.2668)	0.86823 (0.3537)	1.27201 (0.5577)	1.76228 (1.2269)
Slightly nonuniform, Eq. (37)	0.00000 (0.0000)	0.01738 (0.0975)	0.07344 (0.1424)	0.17549 (0.2096)	0.33280 (0.3004)	0.55718 (0.4417)	0.86290 (0.6524)	1.26376 (1.0201)	1.75295 (1.7498)
First-order, eq. (38)	0.00000 (0.0000)	0.01739 (0.0970)	0.07355 (0.1362)	0.17577 (0.1939)	0.33339 (0.2674)	0.55820 (0.3845)	0.86444 (0.5661)	1.26542 (0.9270)	1.75143 (1.8350)
Second-order, eq. (39)	0.00000 (0.0000)	0.01742 (0.0953)	0.07371 (0.1272)	0.17623 (0.1681)	0.33440 (0.2107)	0.56013 (0.2763)	0.86788 (0.3733)	1.27135 (0.5947)	1.76105 (1.2958)

Table 2e. Comparison of deflections calculated from SPAR with those calculated from different deflection equations; tapered cantilever tubular beam; c_n / c_0 = 0.5/4; n = 8.

Theories	y_0 (error, percent)	y_1 (error, percent)	y_2 (error, percent)	y_3 (error, percent)	y_4 (error, percent)	y_5 (error, percent)	y_6 (error, percent)	y_7 (error, percent)	y_8 (error, percent)
SPAR (reference)	0.00000 (0.0000)	0.01938 (0.0000)	0.07872 (0.0000)	0.19047 (0.0000)	0.37082 (0.0000)	0.64535 (0.0000)	1.05517 (0.0000)	1.67290 (0.0000)	2.59712 (0.0000)
Nonuniform, eq. (36)	0.00000 (0.0000)	0.01775 (0.0627)	0.07665 (0.0797)	0.18790 (0.0990)	0.36790 (0.1124)	0.64197 (0.1371)	1.05147 (0.1425)	1.66633 (0.2530)	2.54871 (1.8640)
Slightly nonuniform, eq. (37)	0.00000 (0.0000)	0.01768 (0.0656)	0.07620 (0.0970)	0.18656 (0.1506)	0.36482 (0.2310)	0.63559 (0.3758)	1.03867 (0.6353)	1.64049 (1.2479)	2.50844 (3.4146)
First-order, eq. (38)	0.00000 (0.0000)	0.01771 (0.0643)	0.07640 (0.0893)	0.18714 (0.1282)	0.36615 (0.1798)	0.63829 (0.2718)	1.04386 (0.4355)	1.64986 (0.8871)	2.51231 (3.2655)
Second-order, eq. (39)	0.00000 (0.0000)	0.01775 (0.0628)	0.07663 (0.0805)	0.18783 (0.1017)	0.36774 (0.1186)	0.64159 (0.1448)	1.05057 (0.1771)	1.66394 (0.3435)	2.54197 (2.1235)

Table 2f. Comparison of deflections calculated from SPAR with those calculated from different deflection equations; tapered cantilever tubular beam; c_n / c_0 = 0.25/4; n = 8.

Theories	y_0 (error, percent)	y_1 (error, percent)	y_2 (error, percent)	y_3 (error, percent)	y_4 (error, percent)	y_5 (error, percent)	y_6 (error, percent)	y_7 (error, percent)	y_8 (error, percent)
SPAR (reference)	0.00000 (0.0000)	0.01952 (0.0000)	0.08017 (0.0000)	0.19668 (0.0000)	0.38984 (0.0000)	0.69566 (0.0000)	1.18157 (0.0000)	2.00286 (0.0000)	3.58289 (0.0000)
Nonuniform, eq. (36)	0.00000 (0.0000)	0.01793 (0.0444)	0.07826 (0.0533)	0.19445 (0.0622)	0.38766 (0.0608)	0.69340 (0.0631)	1.17872 (0.1103)	2.00100 (0.0519)	3.43492 (4.1299)
Slightly nonuniform, eq. (37)	0.00000 (0.0000)	0.01785 (0.0466)	0.07771 (0.0687)	0.19276 (0.1094)	0.38359 (0.1744)	0.68447 (0.3123)	1.15879 (0.6358)	1.95019 (1.4700)	3.32381 (7.2310)
First-order, eq. (38)	0.00000 (0.0000)	0.01789 (0.0455)	0.07796 (0.0617)	0.19354 (0.1216)	0.38546 (0.1222)	0.68850 (0.1998)	1.16756 (0.3910)	1.97136 (0.8792)	3.34045 (6.7666)
Second-order, eq. (39)	0.00000 (0.0000)	0.01793 (0.0444)	0.07824 (0.0539)	0.19436 (0.0648)	0.38743 (0.0673)	0.69284 (0.0787)	1.17719 (0.1222)	1.99555 (0.2040)	3.40914 (4.8494)

Note from tables 2a–f that the deflections predicted from the four deflection equations (36)–(39) are fairly close. Note also that the SPAR program provided slightly larger deflections than the corresponding deflections predicted from the four deflection equations. The reason for this difference is that the SPAR deflections contain additional deflection components of transverse shear, which are neglected in the formulation of deflection equations (36)–(39) (see graphical demonstrations in reference 2, figures 17 and 19). Also note that the prediction accuracy of deflection equations (36) and (39) are slightly better than the comparable accuracy of deflection equations (37) and (38).

The deflection data of tables 2a–f calculated from deflection equations (36)–(40) are plotted in figures 5a–d, respectively, for different tapered cantilever tubular beams, and are compared with the corresponding deflection curves calculated from the SPAR program. The small prediction errors shown in tables 2a–f are almost inconspicuous for depth ratio range, $4/4 \geq c_n / c_0 \geq 1/4$. For the cases of low depth ratios, c_n / c_0 = (0.5/4, 0.25/4), however, the predicted deflection curves near the beam tip regions show slight deviations from the corresponding SPAR deflection curves because of the insufficient strain data points used. As discussed in the section entitled, "Domain Density," the shape prediction accuracy near the beam tip regions could be greatly improved by increasing the domain density (increasing the

number of strain stations). Overall, the good graphical correlations between the predicted and SPAR-generated deflection curves provide confidence in the high accuracy of deflection equations (36)–(39) formulated for the nonuniform cantilever beam.

Error Curves

Figure 6 shows the beam tip prediction errors (tables 2a–f) based on different deflection equations plotted as functions of depth ratio, c_n / c_0. For the uniform beam case ($c_n / c_0 = 4/4$), the deflections calculated from deflection equations (37)–(39) are identical, indicating the mathematical accuracy of deflection equations (37)–(39) at the limit of the uniform beam case. For the tapered beam cases, all the deflection equations (36)–(39) predicted reasonably close deflections (a prediction error of approximately 1 percent) in the region of the depth ratios, $3/4 \geq c_n / c_0 \geq 2/4$. As the beam depth ratio decreases from $c_n / c_0 = 2/4$, the prediction errors continue to increase and reach a respective maximum at the lowest depth ratio, $c_n / c_0 = 0.25/4$. The beam tip shape prediction errors at $c_n / c_0 = 0.25/4$ of both the nonuniform deflection equation (36) and second-order deflection equation (39) are comparable, and are nearly 60 percent of the prediction errors of both the slightly nonuniform deflection equation (37) and the first-order deflection equation (38).

DOMAIN DENSITY

As shown in figure 4, as the beam depth ratio, c_n / c_0, decreases, the strain curve continues to bend more and reaches a sharp bend near the beam tip region for the lowest depth ratio, $c_n / c_0 = 0.25/4$. To obtain more accurate strain curves with a piecewise linear approximation (eq. (5)), the strain data points must be increased. Increasing the domain density, n, implies increasing the number $(1 + n)$ of strain stations. Therefore, the domain density, n, was increased from $n = 8$ to $n = 16$ to obtain additional strain data points for generating more accurate strain curves, thereby achieving better shape predictions.

Improved Strain Curves

Figure 7 compares the SPAR-generated strain curves based on the domain densities of $n = 8$ and $n = 16$. For the depth ratios, $c_n / c_0 = 4/4–1/4$, the effect of increasing the domain density, n, is practically inconspicuous. Increasing the value of n, however, has a marked effect on improving the strain curves near the beam tip regions especially for the lower depth cases, $c_n / c_0 = 0.5/4$ and $c_n / c_0 = 0.25/4$. Again, the nonzero strains at the free beam tip are caused by discretization of the beam (theoretically, the free beam tip strain should be zero).

Improved Deflection Data

As shown in figure 7, the beam deflections were recalculated from only deflection equations (36) and (39) (fig. 6) for different tapered tubular beams using the strains based on $n = 16$. Tables 3a–f list the results, with prediction errors indicated in parentheses.

Table 3a. Comparison of deflections calculated from SPAR with those calculated from different deflection equations; uniform cantilever tubular beam; c_n / c_0 = 4/4; n = 16.

Theories	y_0 (error, percent)	y_2 (error, percent)	y_4 (error, percent)	y_6 (error, percent)	y_8 (error, percent)	y_{10} (error, percent)	y_{12} (error, percent)	y_{14} (error, percent)	y_{16} (error, percent)
SPAR (reference)	0.00000 (0.0000)	0.01787 (0.0000)	0.06340 (0.0000)	0.13368 (0.0000)	0.22450 (0.0000)	0.33181 (0.0000)	0.45174 (0.0000)	0.57933 (0.0000)	0.71162 (0.0000)
Nonuniform, eq. (36)	------	------	------	------	------	------	------	------	------
Second-order, eq. (39)	0.00000 (0.0000)	0.01576 (0.2965)	0.06034 (0.4300)	0.12962 (0.5705)	0.21948 (0.7055)	0.32580 (0.8446)	0.44448 (1.0202)	0.57139 (1.1158)	0.70243 (1.2914)

Table 3b. Comparison of deflections calculated from SPAR with those calculated from different deflection equations; tapered cantilever tubular beam; c_n / c_0 = 3/4; n = 16.

Theories	y_0 (error, percent)	y_2 (error, percent)	y_4 (error, percent)	y_6 (error, percent)	y_8 (error, percent)	y_{10} (error, percent)	y_{12} (error, percent)	y_{14} (error, percent)	y_{16} (error, percent)
SPAR (reference)	0.00000 (0.0000)	0.01823 (0.0000)	0.06697 (0.0000)	0.14572 (0.0000)	0.25204 (0.0000)	0.38294 (0.0000)	0.53428 (0.0000)	0.70092 (0.0000)	0.87634 (0.0000)
Nonuniform, eq. (36)	0.00000 (0.0000)	0.01627 (0.2237)	0.06417 (0.3195)	0.14199 (0.4256)	0.24738 (0.5318)	0.37726 (0.6482)	0.52758 (0.7645)	0.69312 (0.8901)	0.86711 (1.0532)
Second-order, eq. (39)	0.00000 (0.0000)	0.01627 (0.2237)	0.06417 (0.3195)	0.14199 (0.4256)	0.24738 (0.5318)	0.37726 (0.6482)	0.52759 (0.7634)	0.69313 (0.8889)	0.86712 (1.0521)

Table 3c. Comparison of deflections calculated from SPAR with those calculated from different deflection equations; tapered cantilever tubular beam; c_n / c_0 = 2/4; n = 16.

Theories	y_0 (error, percent)	y_2 (error, percent)	y_4 (error, percent)	y_6 (error, percent)	y_8 (error, percent)	y_{10} (error, percent)	y_{12} (error, percent)	y_{14} (error, percent)	y_{16} (error, percent)
SPAR (reference)	0.00000 (0.0000)	0.01864 (0.0000)	0.07113 (0.0000)	0.16057 (0.0000)	0.28831 (0.0000)	0.45510 (0.0000)	0.65965 (0.0000)	0.89759 (0.0000)	1.15801 (0.0000)
Nonuniform, eq. (36)	0.00000 (0.0000)	0.01682 (0.1572)	0.06859 (0.2193)	0.15719 (0.2919)	0.28407 (0.3661)	0.44983 (0.4551)	0.65325 (0.5527)	0.88981 (0.6718)	1.14828 (0.8402)
Second-order, eq. (39)	0.00000 (0.0000)	0.01682 (0.1572)	0.06859 (0.2193)	0.15719 (0.2919)	0.28407 (0.3661)	0.44983 (0.4551)	0.65324 (0.5535)	0.88980 (0.6727)	1.14826 (0.8420)

Table 3d. Comparison of deflections calculated from SPAR with those calculated from different deflection equations; tapered cantilever tubular beam; c_n / c_0 = 1/4; n = 16.

Theories	y_0 (error, percent)	y_2 (error, percent)	y_4 (error, percent)	y_6 (error, percent)	y_8 (error, percent)	y_{10} (error, percent)	y_{12} (error, percent)	y_{14} (error, percent)	y_{16} (error, percent)
SPAR (reference)	0.00000 (0.0000)	0.01912 (0.0000)	0.07598 (0.0000)	0.17923 (0.0000)	0.33816 (0.0000)	0.56506 (0.0000)	0.87454 (0.0000)	1.28196 (0.0000)	1.78417 (0.0000)
Nonuniform, eq. (36)	0.00000 (0.0000)	0.01739 (0.0970)	0.07364 (0.1312)	0.17612 (0.1743)	0.33427 (0.2180)	0.56011 (0.2774)	0.86835 (0.3469)	1.27375 (0.4602)	1.77114 (0.7303)
Second-order, eq. (39)	0.00000 (0.0000)	0.01739 (0.0970)	0.07364 (0.1312)	0.17611 (0.1749)	0.33426 (0.2186)	0.56009 (0.2786)	0.86829 (0.3503)	1.27365 (0.4658)	1.77124 (0.7247)

Table 3e. Comparison of deflections calculated from SPAR with those calculated from different deflection equations; tapered cantilever tubular beam; c_n / c_0 = 0.5/4; n = 16.

Theories	y_0 (error, percent)	y_2 (error, percent)	y_4 (error, percent)	y_6 (error, percent)	y_8 (error, percent)	y_{10} (error, percent)	y_{12} (error, percent)	y_{14} (error, percent)	y_{16} (error, percent)
SPAR (reference)	0.00000 (0.0000)	0.01938 (0.0000)	0.07872 (0.0000)	0.19047 (0.0000)	0.37082 (0.0000)	0.64535 (0.0000)	1.05517 (0.0000)	1.67292 (0.0000)	2.59712 (0.0000)
Nonuniform, eq. (36)	0.00000 (0.0000)	0.01770 (0.0647)	0.07649 (0.0859)	0.18752 (0.1136)	0.36721 (0.1390)	0.64077 (0.1763)	1.04963 (0.2133)	1.66517 (0.2984)	2.57675 (0.7843)
Second-order, eq. (39)	0.00000 (0.0000)	0.01770 (0.0647)	0.07648 (0.0862)	0.18751 (0.1140)	0.36719 (0.1398)	0.64071 (0.1787)	1.04949 (0.2187)	1.66478 (0.3134)	2.57544 (0.8348)

Table 3f. Comparison of deflections calculated from SPAR with those calculated from different deflection equations; tapered cantilever tubular beam; c_n / c_0 = 0.25/4; n = 16.

Theories	y_0 (error, percent)	y_2 (error, percent)	y_4 (error, percent)	y_6 (error, percent)	y_8 (error, percent)	y_{10} (error, percent)	y_{12} (error, percent)	y_{14} (error, percent)	y_{16} (error, percent)
SPAR (reference)	0.00000 (0.0000)	0.01952 (0.0000)	0.08017 (0.0000)	0.19668 (0.0000)	0.38984 (0.0000)	0.69566 (0.0000)	1.18157 (0.0000)	2.00286 (0.0000)	3.58289 (0.0000)
Nonuniform, eq. (36)	0.00000 (0.0000)	0.01786 (0.0463)	0.07802 (0.0600)	0.19387 (0.0784)	0.38651 (0.0929)	0.69143 (0.1181)	1.17563 (0.1658)	1.99425 (0.2403)	3.53790 (1.2557)
Second-order, eq. (39)	0.00000 (0.0000)	0.01786 (0.0463)	0.07801 (0.0603)	0.19385 (0.0790)	0.38648 (0.0938)	0.69135 (0.1203)	1.17539 (0.1725)	1.99331 (0.2665)	3.53116 (1.4438)

The deflection data shown in tables 3a–f are plotted in figure 8. Notice from figures 8a and 8b that the beam tip prediction errors using n = 16 did indeed decrease from those using n = 8 (tables 2a–f)), especially for the lower depth ratio cases, c_n / c_0 = 0.25/4, 0.5/4.

Error Comparisons

Tables 4a–f compare the beam tip prediction errors based on n = 8 and n = 16.

Table 4a. Comparison of beam tip prediction errors based on different deflection equations using strain station densities (n = 8, 16); tapered cantilever tubular beam; c_n / c_0 = 4/4.

Theories	n = 8		n = 16		
	y_n, in.	Error, percent	y_n, in.	Error, percent	Error, percent of n = 8
SPAR	0.71162	0.00	0.71162	0.00	0
Nonuniform, eq. (36)	---	---	---	---	---
Second-order, eq. (39)	0.70230	1.31	0.70243	1.29	98

Table 4b. Comparison of beam tip prediction errors based on different deflection equations using strain station densities (n = 8, 16); tapered cantilever tubular beam; c_n / c_0 = 3/4.

Theories	n = 8		n = 16		
	y_n, in.	Error, percent	y_n, in.	Error, percent	Error, percent of n = 8
SPAR	0.87634	0.00	0.87634	0.00	0
Nonuniform, eq. (36)	0.86568	1.22	0.86711	1.05	86
Second-order, eq. (39)	0.86567	1.22	0.86712	1.05	86

Table 4c. Comparison of beam tip prediction errors based on different deflection equations using strain station densities (n = 8, 16); tapered cantilever tubular beam; c_n / c_0 = 2/4.

Theories	n = 8		n = 16		
	y_n, in.	Error, percent	y_n, in.	Error, percent	Error, percent of n = 8
SPAR	1.15801	0.00	1.15801	0.00	0
Nonuniform, eq. (36)	1.14592	1.04	1.14828	0.84	81
Second-order, eq. (39)	1.14518	1.1	1.14827	0.84	76

Table 4d. Comparison of beam tip prediction errors based on different deflection equations using strain station densities (n = 8, 16); tapered cantilever tubular beam; c_n / c_0 = 1/4.

Theories	n = 8		n = 16		
	y_n, in.	Error, percent	y_n, in.	Error, percent	Error, percent of n = 8
SPAR	1.78417	0.00	1.78417	0.00	0
Nonuniform, eq. (36)	1.76228	1.23	1.77144	0.71	58
Second-order, eq. (39)	1.76105	1.30	1.77124	0.72	55

Table 4e. Comparison of beam tip prediction errors based on different deflection equations using strain station densities (n = 8, 16); tapered cantilever tubular beam; c_n / c_0 = 0.5/4.

Theories	n = 8		n = 16		
	y_n, in.	Error, percent	y_n, in.	Error, percent	Error, percent of n = 8
SPAR	2.59712	0.00	2.59712	0.00	0
Nonuniform, eq. (36)	2.54871	1.86	2.57675	0.78	42
Second-order, eq. (39)	2.54197	2.12	2.57544	0.83	39

Table 4f. Comparison of beam tip prediction errors based on different deflection equations using strain station densities (n = 8, 16); tapered cantilever tubular beam; c_n / c_0 = 0.25/4.

Theories	n = 8		n = 16		
	y_n, in.	Error, percent	y_n, in.	Error, percent	Error, percent of n = 8
SPAR	3.58289	0.00	3.58289	0.00	0
Nonuniform, eq. (36)	3.43492	4.13	3.53790	1.26	31
Second-order, eq. (39)	3.40914	4.85	3.52116	1.44	30

Figure 9 plots the beam tip deflection prediction errors based on n = 8 and n = 16 (tables 4a–f) for comparison. Note that the effect of increasing the domain density, n, on the reduction of prediction errors becomes more conspicuous as the depth ratio, c_n / c_0, decreases. At the lowest depth ratio, c_n / c_0 = 0.25/4, the beam tip prediction errors based on n = 16 were reduced to almost 30 percent of those based on n = 8.

DISCUSSION

For the present shape predictions of the tapered cantilever tubular beam, all four displacement transfer functions (deflection equations (36)–(39)) were found to provide quite accurate shape predictions. The slightly nonuniform deflection equation (37) and the first-order deflection equation (38) have comparable prediction accuracy and are recommended for shape predictions of slightly nonuniform beam cases. For shape predictions of nonuniform beam structures, both the exact deflection equation (36) and second-order deflection equation (39) can be used, because both deflection equations can provide comparable shape prediction accuracy.

Note that when the fiber-optic strain-sensing system is used, off-the-shelf sensor density is high, thereby improving shape prediction accuracy. This high sensor density can be decimated by an integer factor to reduce computational requirements while sacrificing prediction accuracy. Thus, for improving shape prediction accuracy, the previously specified number (n + 1) of strain data extraction points can be increased as desired, up to a level corresponding to the off-the-shelf sensor density, by means of a simple command. By increasing the domain density, n, the assumed piecewise-linear strain curves will approach the associated true smooth strain curves (especially for the highly tapered beam tip region where the bending strains reach a maximum and then drop rapidly toward the beam tip), and thus greatly improve the shape prediction accuracy.

SUMMARY

The first- and the second-order displacement transfer functions were formulated for the nonuniform cantilever beam through binomial series expansions of the beam depth function. The principal results are as follows:

1. Through binomial series expansions of the axially varying beam depth function, the mathematical indeterminacy problem at the limit case of a uniform beam was successfully eliminated.

2. The deflections calculated from all four displacement transfer functions were reasonably close and were slightly lower than the corresponding deflections generated by the Structural Performance

And Resizing (SPAR) program. The SPAR-generated deflections contained additional components induced by the transverse shear effect, which was ignored in the analysis.

3. For the uniform beam case (c_n / c_0 = 4/4), the deflections predicted from different displacement transfer functions were identical, confirming the mathematical accuracy of all the displacement transfer functions formulated.

4. The shape prediction accuracy of the nonuniform and second-order displacement transfer functions were slightly better than the comparable accuracy of both the slightly nonuniform and first-order displacement transfer functions.

5. For the tapered beam shape predictions, using the second-order displacement transfer function instead of the first-order deflection equation did not change the beam tip prediction error for the uniform beam (zero taper angle). For the tapered beam, however, the prediction error continued to decrease with increasing taper angle, reaching a 28-percent error reduction at the peak taper angle.

6. For the tapered beam shape predictions, using the nonuniform displacement transfer function instead of the slightly nonuniform deflection equation decreased the beam tip prediction errors with increasing taper angle, reaching a 43-percent error reduction at the peak taper angle.

7. For the tapered beam, the shape prediction accuracy could be improved by increasing the domain density. By doubling the domain density, one could reduce the average beam tip prediction errors by 2 percent at a zero taper angle (uniform beam). The error reduction continued to improve with increasing taper angle, reaching a 69-percent error reduction at the peak taper angle.

FIGURES

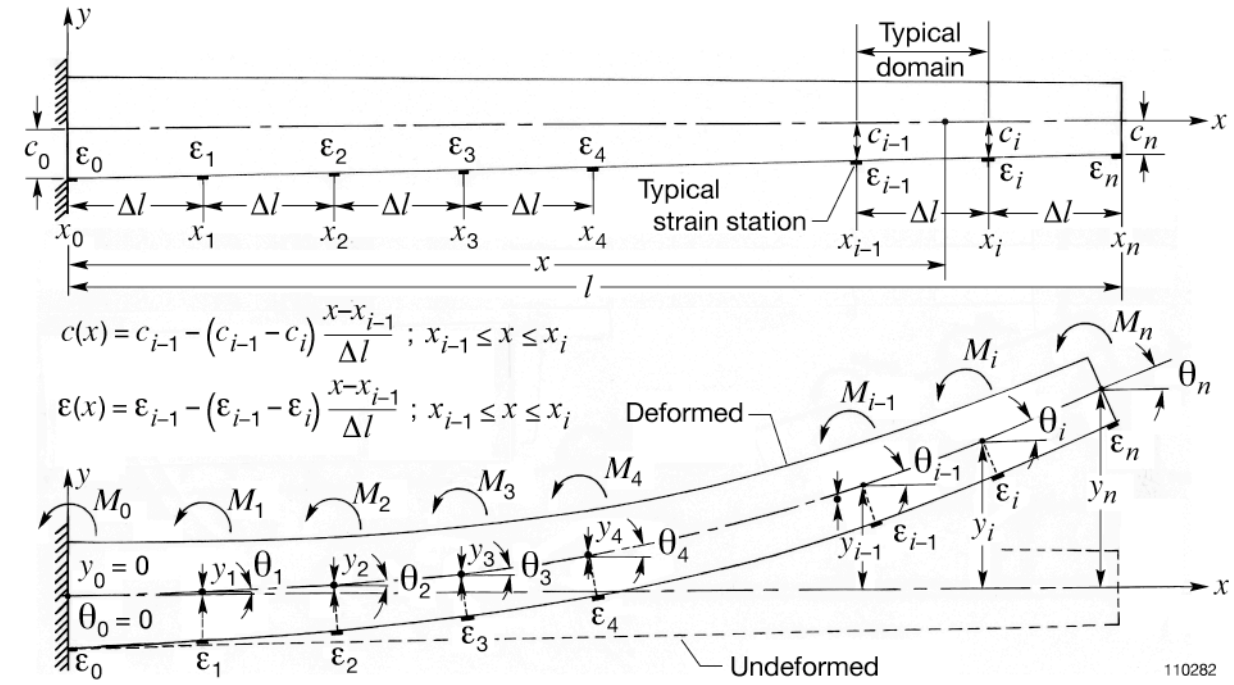

Figure 1. Nonuniform cantilever beam instrumented with equally spaced surface bending strain sensors.

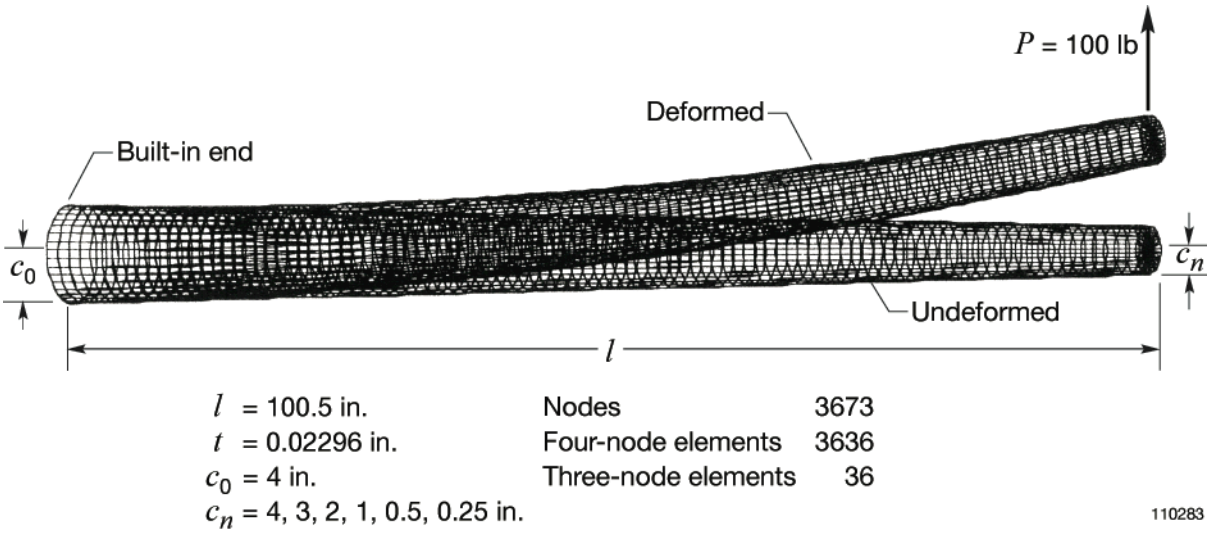

Figure 2. Finite-element model for tapered cantilever tubular beam subjected to a tip vertical load of P = 100 lb.

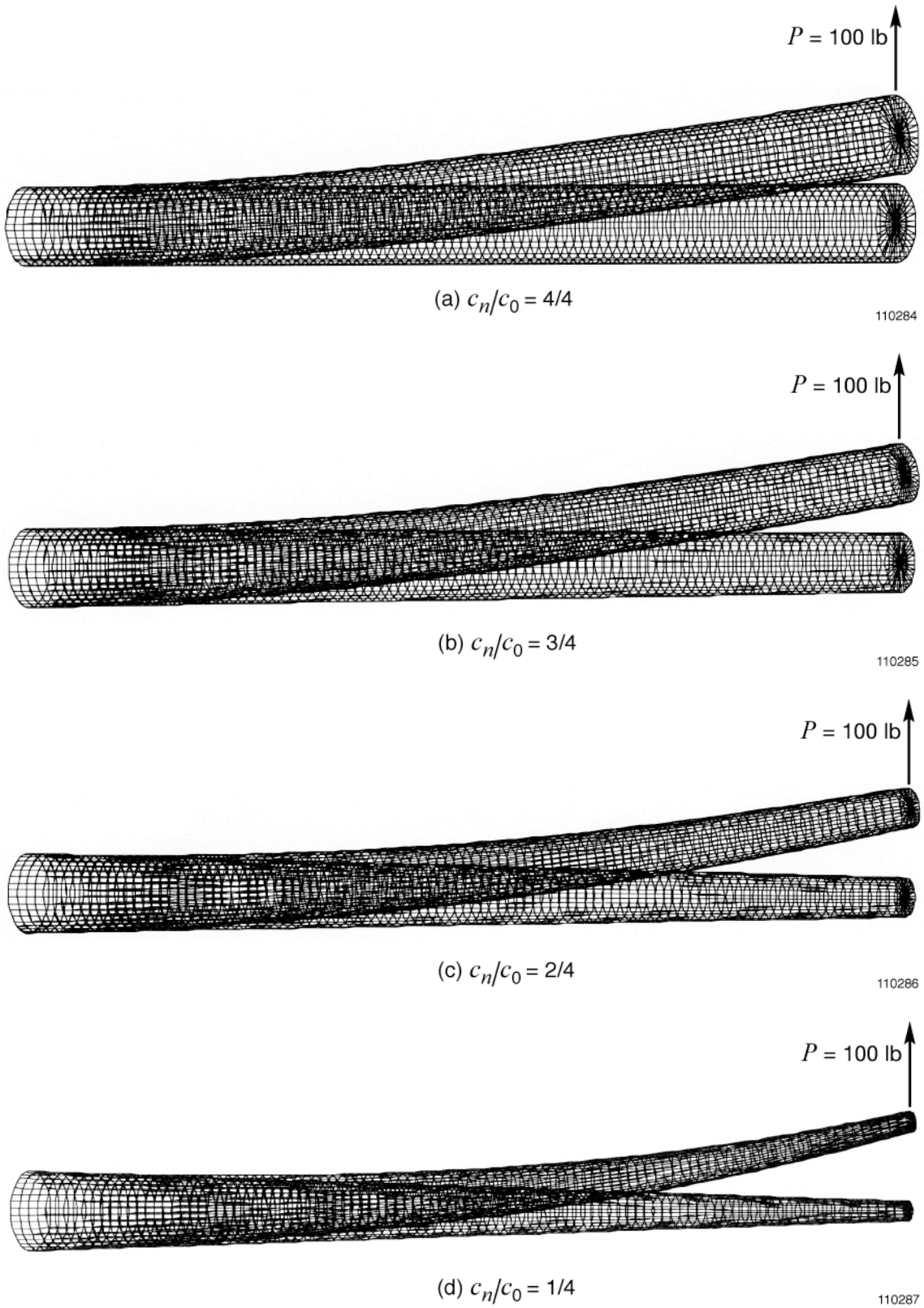

Figure 3. Deformed shapes, generated from the Structural Performance And Resizing (SPAR) program, of different tapered cantilever tubular beams; P = 100 lb.

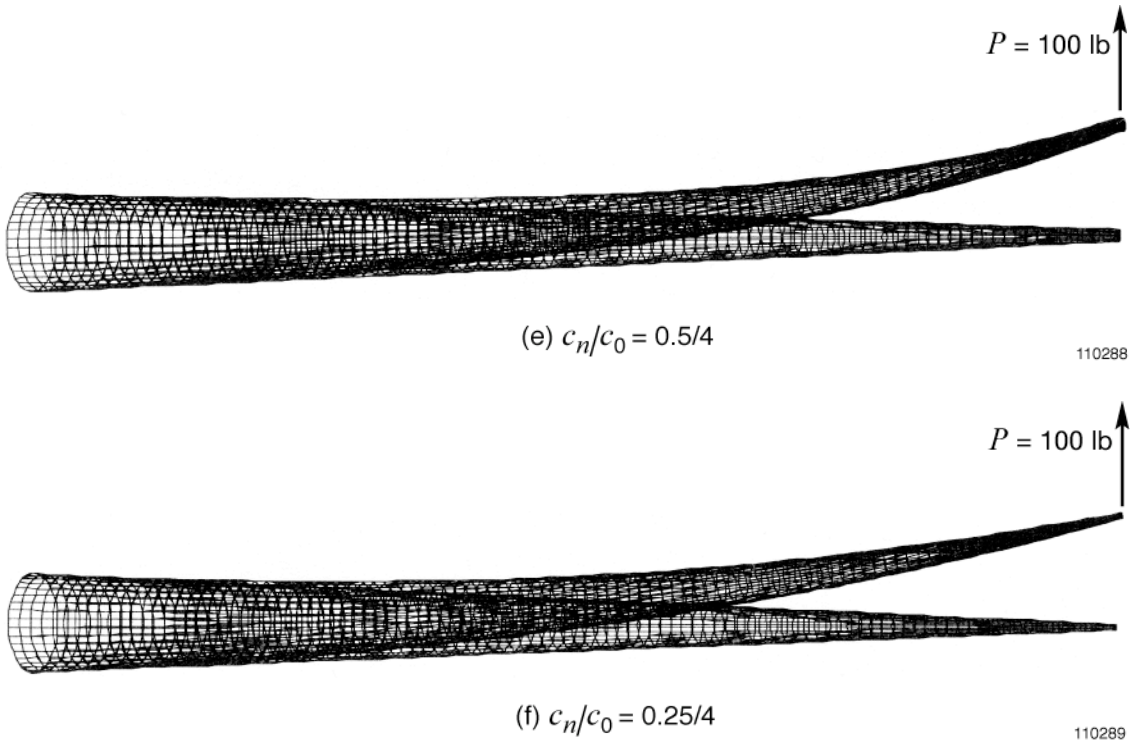

Figure 3. Concluded.

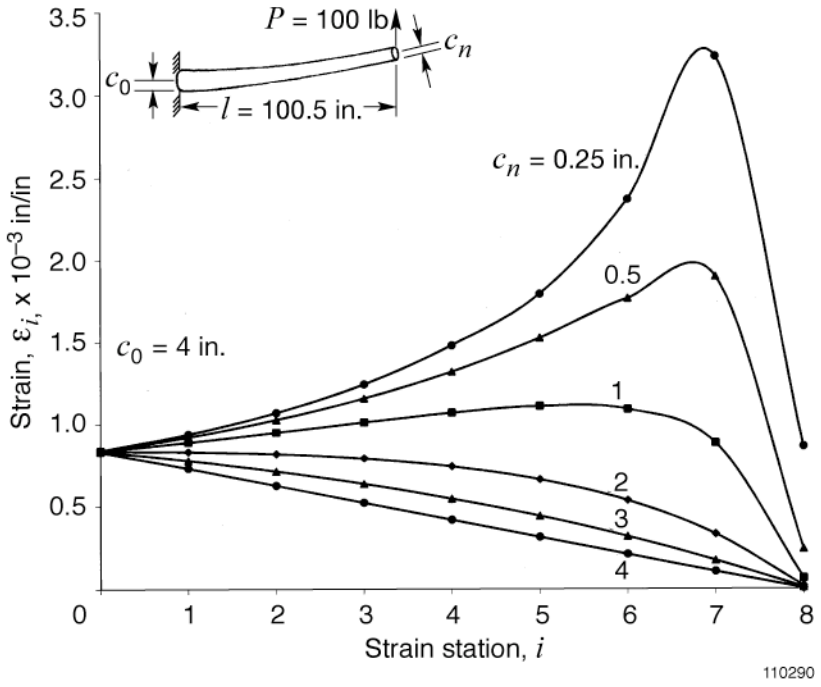

Figure 4. Surface bending strains calculated from the Structural Performance And Resizing (SPAR) element stress outputs for different tapered cantilever tubular beams; n = 8; P = 100 lb.

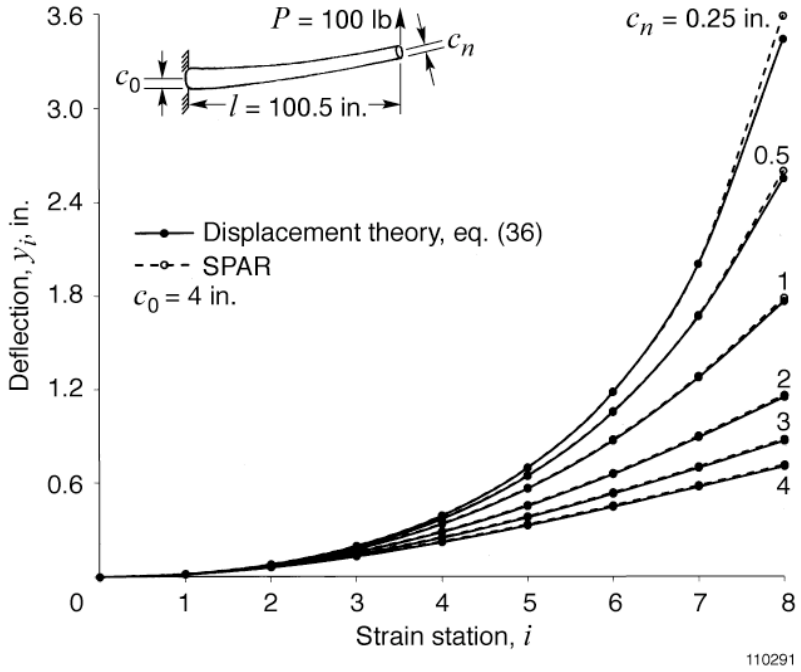

(a) Deflections calculated from deflection equation (36), for nonuniform beams, compared with those calculated from SPAR (deflection equation (40) was used for the uniform beam).

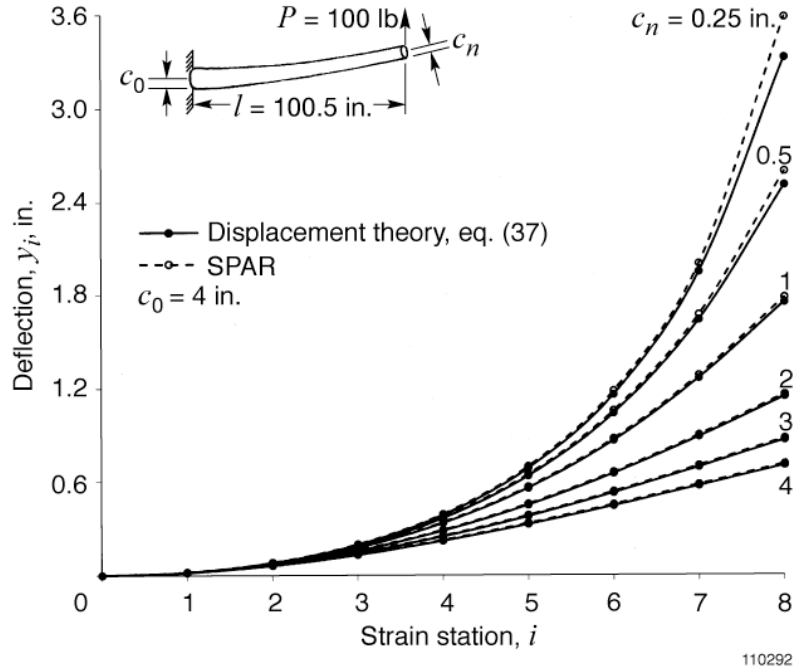

(b) Deflections calculated from deflection equation (37), for slightly nonuniform beams, compared with those calculated from SPAR (deflection equation (40) was used for the uniform beam).

Figure 5. Comparison of deflections calculated from deflection equations with those calculated from the Structural Performance And Resizing (SPAR) program for different tapered cantilever tubular beams; n = 8; P = 100 lb.

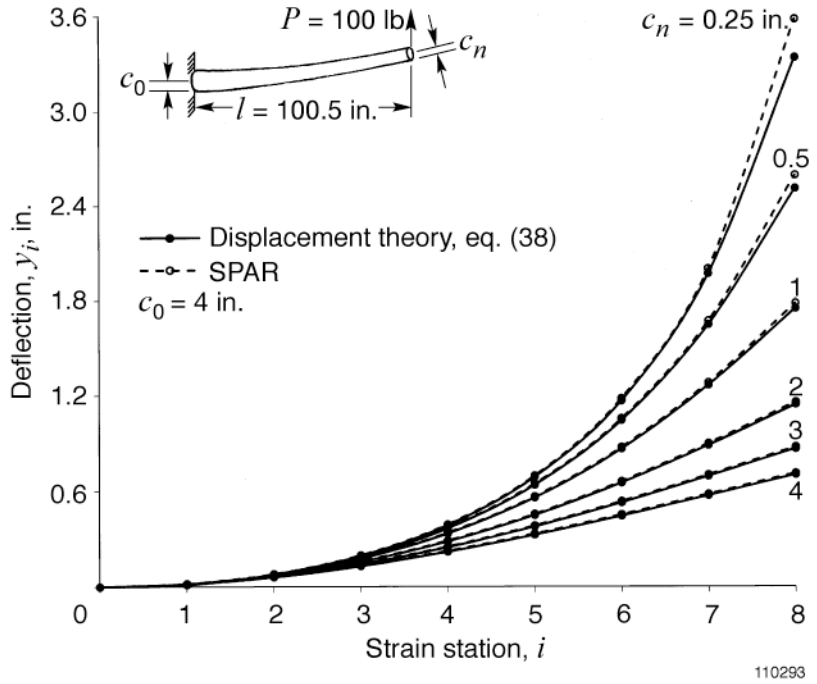

(c) Deflections calculated from first-order deflection equation (38) compared with those calculated from SPAR (deflection equation (40) was used for the uniform beam).

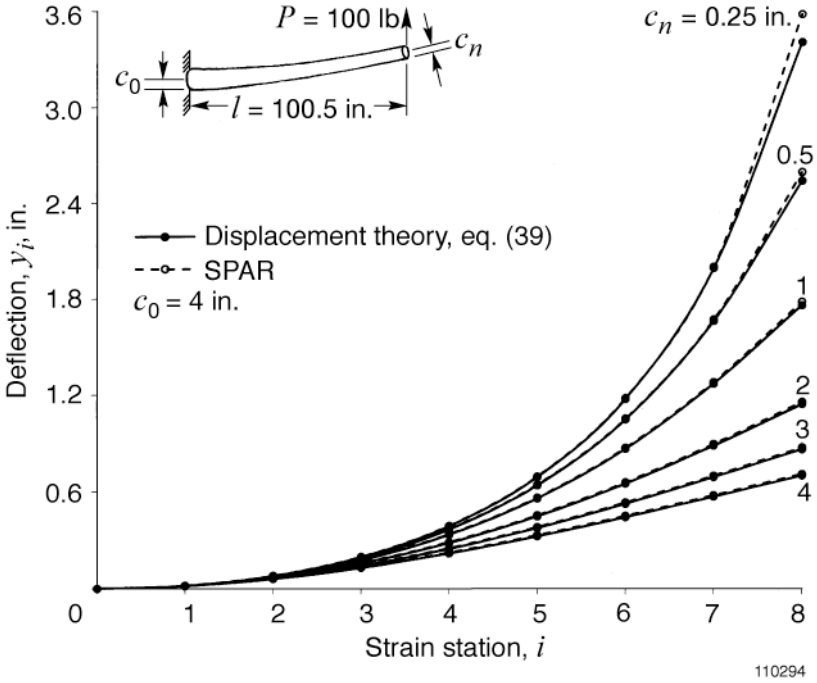

(d) Deflections calculated from second-order deflection equation (39) compared with those calculated from SPAR (deflection equation (40) was used for the uniform beam).

Figure 5. Concluded.

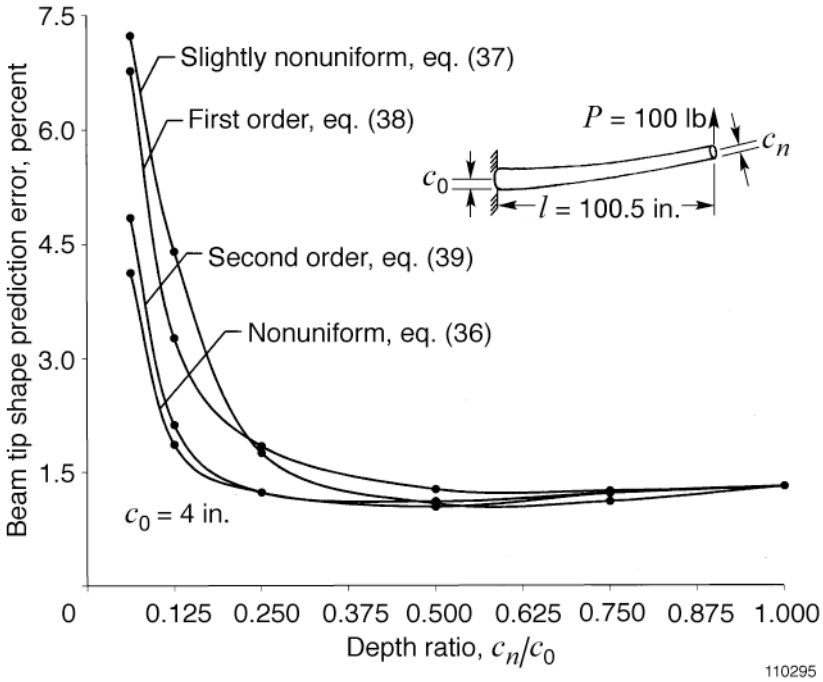

Figure 6. Beam tip deflection prediction errors associated with different displacement transfer functions plotted as functions of depth ratio, c_n / c_0.

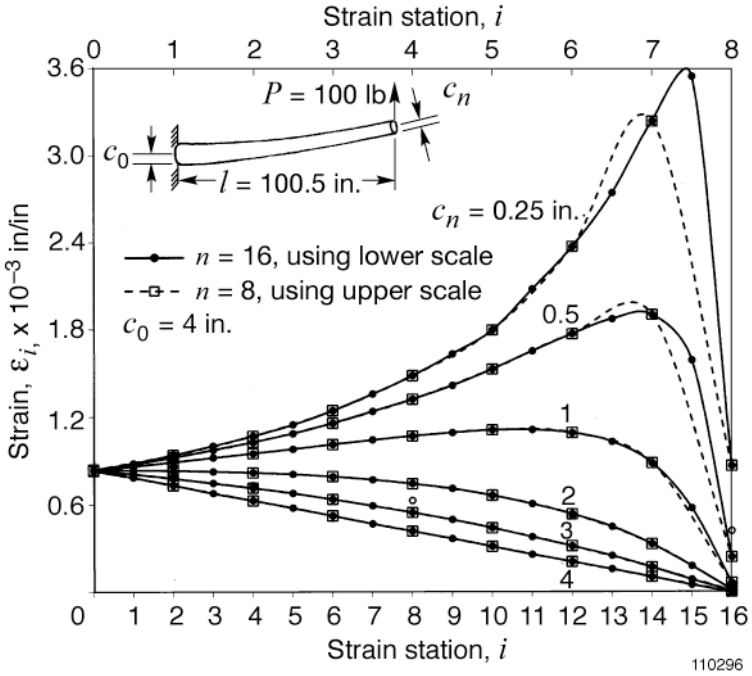

Figure 7. Comparison of bending strain curves for different tapered cantilever tubular beams based on $n = 8$ and $n = 16$; $P = 100$ lb.

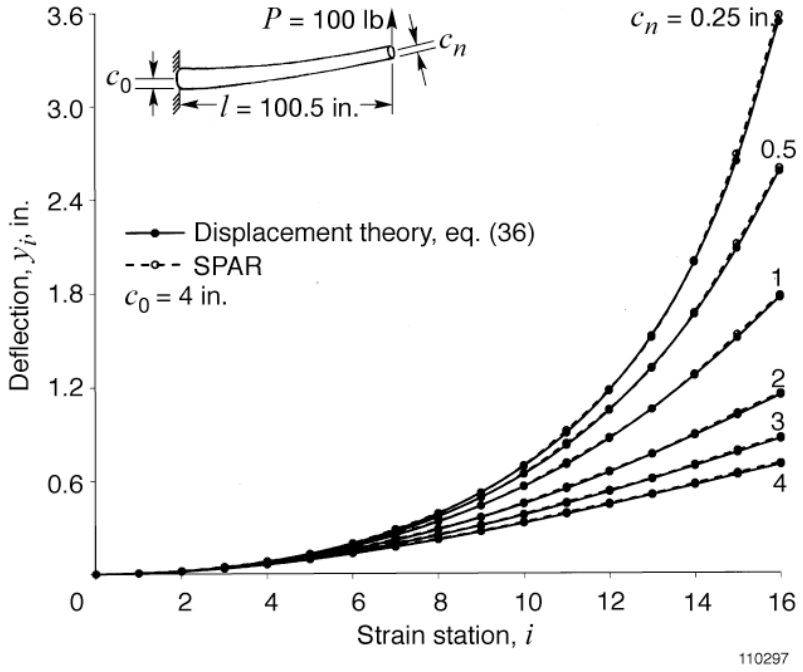

(a) Deflections calculated from deflection equation (36), for nonuniform beams, compared with those calculated from SPAR (deflection equation (40) was used for the uniform beam).

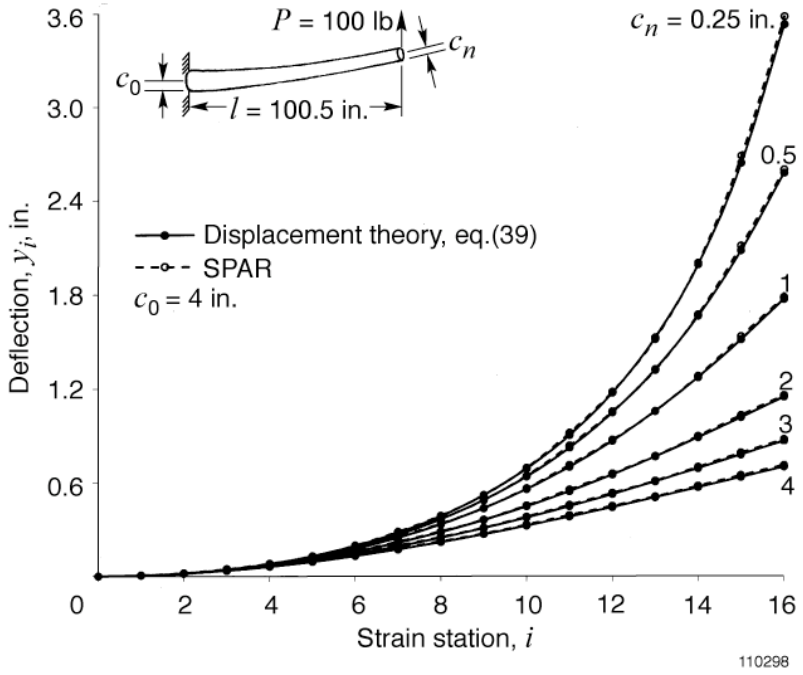

(b) Deflections calculated from second-order deflection equation (39) compared with those calculated from SPAR.

Figure 8. Comparison of deflections calculated from deflection equations with those calculated from the Structural Performance And Resizing (SPAR) program for different tapered cantilever tubular beams; n = 16; P = 100 lb.

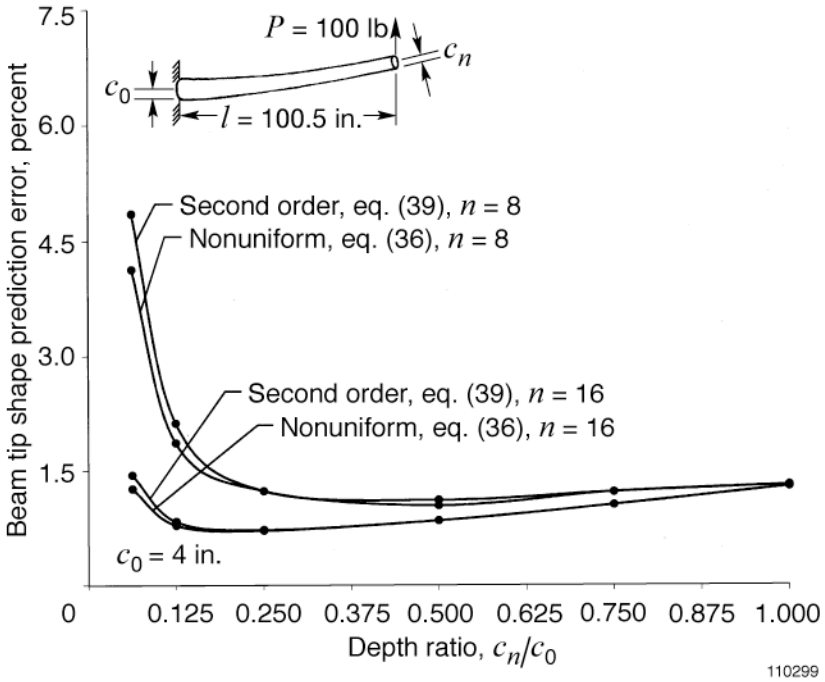

Figure 9. Comparison of beam tip deflection prediction error curves associated with different displacement functions based on n = 8 and n = 16.

APPENDIX A

DERIVATIONS OF THE FIRST-ORDER SLOPE AND DEFLECTION EQUATIONS

Appendix A presents the detailed mathematical derivations of the first-order slope equations and first-order deflection equations for the nonuniform cantilever beam.

Basic Slope Equations

The slope, $\tan\theta(x)(\equiv dy/dx)$, of the nonuniform beam at the axial location, x, within the domain, $x_{i-1} \le x \le x_i$ (fig. 1), can be obtained by integrating the beam differential equation (3) once, and enforcing the continuity of the slope at the inboard strain station, x_{i-1}, as

$$\tan\theta(x) = \underbrace{\int_{x_{i-1}}^{x} \frac{d^2y}{dx^2}dx}_{\text{Integration of eq. (3)}} + \underbrace{\tan\theta_{i-1}}_{\text{Slope at } x_{i-1}} = \underbrace{\int_{x_{i-1}}^{x} \frac{\varepsilon(x)}{c(x)}dx}_{\substack{\text{Slope increment} \\ \text{above } \tan\theta_{i-1}}} + \underbrace{\tan\theta_{i-1}}_{\text{Slope at } x_{i-1}} \quad ; \quad (x_{i-1} \le x \le x_i) \tag{A1}$$

in which $\tan\theta_{i-1}$ is the slope at the inboard strain station, x_{i-1}.

In light of the following linear assumptions of both $c(x)$ and $\varepsilon(x)$ within the domain, $x_{i-1} \le x \le x_i$,

$$c(x) = c_{i-1} - (c_{i-1} - c_i)\frac{x - x_{i-1}}{\Delta l} \quad ; \quad (x_{i-1} \le x \le x_i) \tag{A2}$$

$$\varepsilon(x) = \varepsilon_{i-1} - (\varepsilon_{i-1} - \varepsilon_i)\frac{x - x_{i-1}}{\Delta l} \quad ; \quad (x_{i-1} \le x \le x_i) \tag{A3}$$

equation (A1) becomes

$$\tan\theta(x) = \frac{\varepsilon_{i-1}}{c_{i-1}} \int_{x_{i-1}}^{x} \frac{1 - \left(1 - \dfrac{\varepsilon_i}{\varepsilon_{i-1}}\right)\dfrac{x - x_{i-1}}{\Delta l}}{1 - \left(1 - \dfrac{c_i}{c_{i-1}}\right)\dfrac{x - x_{i-1}}{\Delta l}} dx + \tan\theta_{i-1} \quad ; \quad (x_{i-1} \le x \le x_i) \tag{A4}$$

First-Order Slope Equations

Because the coefficient, $1-(c_i / c_{i-1})$, of the slope term in the denominator of equation (A4) is considered small, one can expand the factor, $\left[1-\left(1-\frac{c_i}{c_{i-1}}\right)\frac{x-x_{i-1}}{\Delta l}\right]^{-1}$, in binomial series up to the first-order term as

$$\tan\theta(x)=\frac{\varepsilon_{i-1}}{c_{i-1}}\int_{x_{i-1}}^{x}\left[1-\left(1-\frac{\varepsilon_i}{\varepsilon_{i-1}}\right)\frac{x-x_{i-1}}{\Delta l}\right]\left[1+\left(1-\frac{c_i}{c_{i-1}}\right)\frac{x-x_{i-1}}{\Delta l}+....\right]dx+\tan\theta_{i-1}$$

$$=\frac{\varepsilon_{i-1}}{c_{i-1}}\int_{x_{i-1}}^{x}\left\{1+\left[\left(1-\frac{c_i}{c_{i-1}}\right)-\left(1-\frac{\varepsilon_i}{\varepsilon_{i-1}}\right)\right]\frac{x-x_{i-1}}{\Delta l}-\left(1-\frac{\varepsilon_i}{\varepsilon_{i-1}}\right)\left(1-\frac{c_i}{c_{i-1}}\right)\frac{(x-x_{i-1})^2}{(\Delta l)^2}+....\right\}dx+\tan\theta_{i-1} \qquad \text{(A5)}$$

After the integration is carried out, equation (A5) becomes

$$\tan\theta(x)=\frac{\varepsilon_{i-1}}{c_{i-1}}\left[(x-x_{i-1})+\left(\frac{\varepsilon_i}{\varepsilon_{i-1}}-\frac{c_i}{c_{i-1}}\right)\frac{(x-x_{i-1})^2}{2\Delta l}-\left(1-\frac{\varepsilon_i}{\varepsilon_{i-1}}\right)\left(1-\frac{c_i}{c_{i-1}}\right)\frac{(x-x_{i-1})^3}{3(\Delta l)^2}\right]+\tan\theta_{i-1}$$

$$(x_{i-1}\le x\le x_i) \qquad \text{(A6)}$$

which is the first-order slope equation for the domain, $x_{i-1}\le x\le x_i$.

At the strain station, $x=x_i$, we have $(x_i-x_{i-1})=\Delta l$, and equation (A6) becomes

$$\tan\theta_i\equiv\tan\theta(x_i)=\frac{\Delta l\varepsilon_{i-1}}{c_{i-1}}\left[1+\frac{1}{2}\left(\frac{\varepsilon_i}{\varepsilon_{i-1}}-\frac{c_i}{c_{i-1}}\right)-\frac{1}{3}\left(1-\frac{\varepsilon_i}{\varepsilon_{i-1}}\right)\left(1-\frac{c_i}{c_{i-1}}\right)\right]+\tan\theta_{i-1}$$

$$=\frac{\Delta l}{6c_{i-1}}\left\{\left[6-3\frac{c_i}{c_{i-1}}-2\left(1-\frac{c_i}{c_{i-1}}\right)\right]\varepsilon_{i-1}+\left[3+2\left(1-\frac{c_i}{c_{i-1}}\right)\right]\varepsilon_i\right\}+\tan\theta_{i-1}$$

$$(i=1,\ 2,\ 3,\ ...,\ n) \qquad \text{(A7)}$$

After the terms are grouped, equation (A7) becomes

$$\tan\theta_i=\frac{\Delta l}{6c_{i-1}}\left[\left(4-\frac{c_i}{c_{i-1}}\right)\varepsilon_{i-1}+\left(5-2\frac{c_i}{c_{i-1}}\right)\varepsilon_i\right]+\tan\theta_{i-1}\ \ ;\ \ (i=1,\ 2,\ 3,\ ...,\ n) \qquad \text{(A8)}$$

Equation (A8) is equation (17) in the main section of this report, and the first-order slope equation is written in descending recursion form. Applying the descending recursion relationships, one can write equation (A8) in summation form as

$$\tan\theta_i = \frac{\Delta l}{6}\sum_{j=1}^{i}\frac{1}{c_{j-1}}\left[\left(4-\frac{c_j}{c_{j-1}}\right)\varepsilon_{j-1}+\left(5-2\frac{c_j}{c_{j-1}}\right)\varepsilon_j\right]+\underbrace{\tan\theta_0}_{\substack{=0 \text{ for canti-}\\ \text{lever beams}}} \quad ; \quad (i=1,\ 2,\ 3,\ ...,\ n) \tag{A9}$$

Equation (A9) is equation (18) in the main section of this report, and the first-order slope equation is written in series summation form.

For the uniform beam ($c_i = c_{i-1} = c$), equation (A9) degenerates into the form

$$\tan\theta_i = \frac{\Delta l}{2c}\sum_{j=1}^{i}(\varepsilon_{j-1}+\varepsilon_j)+\underbrace{\tan\theta_0}_{\substack{=0 \text{ for canti-}\\ \text{lever beams}}} \quad ; \quad (i=1,\ 2,\ 3,\ ...,\ n) \tag{A10}$$

which is identical to equation (25) of reference 2.

First-Order Deflection Equations

The deflection, $y(x)$, at the axial location, x, within the domain, $x_{i-1} \le x \le x_i$ (fig. 1), can be obtained by integrating equation (A6) and enforcing the continuity of the deflection at the inboard strain station, x_{i-1}. Namely,

$$\begin{aligned} y(x) &= \int_{x_{i-1}}^{x} \underbrace{\tan\theta(x)}_{\text{Eq. (A6)}}dx + y_{i-1} \\ &= \frac{\varepsilon_{i-1}}{c_{i-1}}\int_{x_{i-1}}^{x}\left[(x-x_{i-1})+\left(\frac{\varepsilon_i}{\varepsilon_{i-1}}-\frac{c_i}{c_{i-1}}\right)\frac{(x-x_{i-1})^2}{2\Delta l}-\left(1-\frac{\varepsilon_i}{\varepsilon_{i-1}}\right)\left(1-\frac{c_i}{c_{i-1}}\right)\frac{(x-x_{i-1})^3}{3(\Delta l)^2}\right]dx \\ &\qquad + \int_{x_{i-1}}^{x}\tan\theta_{i-1}\,dx + y_{i-1} \end{aligned}$$

$$(x_{i-1} \le x \le x_i) \tag{A11}$$

in which y_{i-1} is the deflection at the inboard strain station, x_{i-1}. After the integration is carried out, equation (A11) becomes

$$y(x) = \frac{\varepsilon_{i-1}}{12c_{i-1}}\left[6(x-x_{i-1})^2 + 2\left(\frac{\varepsilon_i}{\varepsilon_{i-1}} - \frac{c_i}{c_{i-1}}\right)\frac{(x-x_{i-1})^3}{\Delta l} - \left(1-\frac{\varepsilon_i}{\varepsilon_{i-1}}\right)\left(1-\frac{c_i}{c_{i-1}}\right)\frac{(x-x_{i-1})^4}{(\Delta l)^2}\right] + (x-x_{i-1})\tan\theta_{i-1} + y_{i-1}$$

$$(x_{i-1} \le x \le x_i) \qquad \text{(A12)}$$

Equation (A12) is the first-order deflection equation for the domain, $x_{i-1} \le x \le x_i$.

At the strain station, $x = x_i$, we have $(x_i - x_{i-1}) = \Delta l$, and equation (A12) takes on the form

$$y_i \equiv y(x_i) = \frac{(\Delta l)^2 \varepsilon_{i-1}}{12c_{i-1}}\left[6 + 2\frac{\varepsilon_i}{\varepsilon_{i-1}} - 2\frac{c_i}{c_{i-1}} - \left(1 - \frac{\varepsilon_i}{\varepsilon_{i-1}} - \frac{c_i}{c_{i-1}} + \frac{c_i}{c_{i-1}}\frac{\varepsilon_i}{\varepsilon_{i-1}}\right)\right] + y_{i-1} + \Delta l \tan\theta_{i-1}$$

$$(i = 1,\ 2,\ 3,\ ...,\ n) \qquad \text{(A13)}$$

After the terms are grouped, equation (A13) becomes

$$y_i = \frac{(\Delta l)^2}{12c_{i-1}}\left[\left(5 - \frac{c_i}{c_{i-1}}\right)\varepsilon_{i-1} + \left(3 - \frac{c_i}{c_{i-1}}\right)\varepsilon_i\right] + y_{i-1} + \Delta l \tan\theta_{i-1} \quad ; \quad (i = 1,\ 2,\ 3,\ ...,\ n) \qquad \text{(A14)}$$

Equation (A14) is equation (21) in the main section of this report, and the first-order deflection equation is written in descending recursion form.

For the uniform beam ($c_i = c_{i-1} = c$), equation (A14) degenerates into

$$y_i = \frac{(\Delta l)^2}{6c}\left(2\varepsilon_{i-1} + \varepsilon_i\right) + y_{i-1} + \Delta l \tan\theta_{i-1} \quad ; \quad (i = 1,\ 2,\ 3,\ ...,\ n) \qquad \text{(A15)}$$

which is identical to equation (26) of reference 2.

Final Form of Equation (A14)

Substituting the slope equation (A8) into deflection equation (A14), and applying the descending indicial recursion relationships, one can write the resulting deflection equation for each index, $i\,(= 1,\ 2,\ 3,\ ...,\ n)$, as follows:

For $i = 1$,

$$y_1 = \frac{(\Delta l)^2}{12}\frac{1}{c_0}\left[\left(5-\frac{c_1}{c_0}\right)\varepsilon_0 + \left(3-\frac{c_1}{c_0}\right)\varepsilon_1\right] + y_0 + \Delta l \tan\theta_0 \tag{A16}$$

For $i = 2$,

$$y_2 = \frac{(\Delta l)^2}{12}\frac{1}{c_1}\left[\left(5-\frac{c_2}{c_1}\right)\varepsilon_1 + \left(3-\frac{c_2}{c_1}\right)\varepsilon_2\right] + \underbrace{\frac{(\Delta l)^2}{12}\frac{1}{c_0}\left[\left(5-\frac{c_1}{c_0}\right)\varepsilon_0 + \left(3-\frac{c_1}{c_0}\right)\varepsilon_1\right] + y_0 + \Delta l \tan\theta_0}_{y_1}$$

$$\underbrace{+\frac{(\Delta l)^2}{6}\frac{1}{c_0}\left[\left(4-\frac{c_1}{c_0}\right)\varepsilon_0 + \left(5-2\frac{c_1}{c_0}\right)\varepsilon_1\right] + \Delta l \tan\theta_0}_{\Delta l \tan\theta_1} \tag{A17}$$

After the terms are grouped, equation (A17) becomes

$$y_2 = \frac{(\Delta l)^2}{12}\left\{\frac{1}{c_1}\left[\left(5-\frac{c_2}{c_1}\right)\varepsilon_1 + \left(3-\frac{c_2}{c_1}\right)\varepsilon_2\right] + \frac{1}{c_0}\left[\left(13-3\frac{c_1}{c_0}\right)\varepsilon_0 + \left(13-5\frac{c_1}{c_0}\right)\varepsilon_1\right]\right\} + y_0 + 2\Delta l \tan\theta_0 \tag{A18}$$

For $i = 3$,

$$y_3 = \frac{(\Delta l)^2}{12}\frac{1}{c_2}\left[\left(5-\frac{c_3}{c_2}\right)\varepsilon_2 + \left(3-\frac{c_3}{c_2}\right)\varepsilon_3\right]$$

$$\underbrace{+\frac{(\Delta l)^2}{12}\frac{1}{c_1}\left[\left(5-\frac{c_2}{c_1}\right)\varepsilon_1 + \left(3-\frac{c_2}{c_1}\right)\varepsilon_2\right] + \frac{(\Delta l)^2}{12}\frac{1}{c_0}\left[\left(13-3\frac{c_1}{c_0}\right)\varepsilon_0 + \left(13-5\frac{c_1}{c_0}\right)\varepsilon_1\right] + y_0 + 2\Delta l \tan\theta_0}_{y_2}$$

$$\underbrace{+\frac{(\Delta l)^2}{6}\frac{1}{c_1}\left[\left(4-\frac{c_2}{c_1}\right)\varepsilon_1 + \left(5-2\frac{c_2}{c_1}\right)\varepsilon_2\right] + \frac{(\Delta l)^2}{6}\frac{1}{c_0}\left[\left(4-\frac{c_1}{c_0}\right)\varepsilon_0 + \left(5-2\frac{c_1}{c_0}\right)\varepsilon_1\right] + \Delta l \tan\theta_0}_{\Delta l \tan\theta_2} \tag{A19}$$

After the terms are grouped, equation (A19) becomes

$$\begin{aligned} y_3 = \frac{(\Delta l)^2}{12}\frac{1}{c_2}\left[\left(5-\frac{c_3}{c_2}\right)\varepsilon_2 + \left(3-\frac{c_3}{c_2}\right)\varepsilon_3\right] + \frac{(\Delta l)^2}{12}\frac{1}{c_1}\left[\left(13-3\frac{c_2}{c_1}\right)\varepsilon_1 + \left(13-5\frac{c_2}{c_1}\right)\varepsilon_2\right] \\ + \frac{(\Delta l)^2}{12}\frac{1}{c_0}\left[\left(21-5\frac{c_1}{c_0}\right)\varepsilon_0 + \left(23-9\frac{c_1}{c_0}\right)\varepsilon_1\right] + y_0 + 3\Delta l \tan\theta_0 \end{aligned} \tag{A20}$$

For $i = 4$,

$$
\begin{aligned}
y_4 = {} & \frac{(\Delta l)^2}{12}\frac{1}{c_3}\left[\left(5-\frac{c_4}{c_3}\right)\varepsilon_3+\left(3-\frac{c_4}{c_3}\right)\varepsilon_4\right] \\
& + \underbrace{\left\{\begin{array}{l}\dfrac{(\Delta l)^2}{12}\dfrac{1}{c_2}\left[\left(5-\dfrac{c_3}{c_2}\right)\varepsilon_2+\left(3-\dfrac{c_3}{c_2}\right)\varepsilon_3\right]+\dfrac{(\Delta l)^2}{12}\dfrac{1}{c_1}\left[\left(13-3\dfrac{c_2}{c_1}\right)\varepsilon_1+\left(13-5\dfrac{c_2}{c_1}\right)\varepsilon_2\right] \\ \quad +\dfrac{(\Delta l)^2}{12}\dfrac{1}{c_0}\left[\left(21-5\dfrac{c_1}{c_0}\right)\varepsilon_0+\left(23-9\dfrac{c_1}{c_0}\right)\varepsilon_1\right]+y_0+3\Delta l\tan\theta_0\end{array}\right\}}_{y_3} \\
& + \underbrace{\left\{\begin{array}{l}\dfrac{(\Delta l)^2}{6}\dfrac{1}{c_2}\left[\left(4-\dfrac{c_3}{c_2}\right)\varepsilon_2+\left(5-2\dfrac{c_3}{c_2}\right)\varepsilon_3\right]+\dfrac{(\Delta l)^2}{6}\dfrac{1}{c_1}\left[\left(4-\dfrac{c_2}{c_1}\right)\varepsilon_1+\left(5-2\dfrac{c_2}{c_1}\right)\varepsilon_2\right] \\ +\dfrac{(\Delta l)^2}{6}\dfrac{1}{c_0}\left[\left(4-\dfrac{c_1}{c_0}\right)\varepsilon_0+\left(5-2\dfrac{c_1}{c_0}\right)\varepsilon_1\right]+\Delta l\tan\theta_0\end{array}\right\}}_{\Delta l\tan\theta_3}
\end{aligned}
\tag{A21}
$$

After the terms are grouped, equation (A21) becomes

$$
\begin{aligned}
y_4 = {} & \frac{(\Delta l)^2}{12}\frac{1}{c_3}\left[\left(5-\frac{c_4}{c_3}\right)\varepsilon_3+\left(3-\frac{c_4}{c_3}\right)\varepsilon_4\right] \\
& +\frac{(\Delta l)^2}{12}\frac{1}{c_2}\left[\left(13-3\frac{c_3}{c_2}\right)\varepsilon_2+\left(13-5\frac{c_3}{c_2}\right)\varepsilon_3\right]+\frac{(\Delta l)^2}{12}\frac{1}{c_1}\left[\left(21-5\frac{c_2}{c_1}\right)\varepsilon_1+\left(23-9\frac{c_2}{c_1}\right)\varepsilon_2\right] \\
& +\frac{(\Delta l)^2}{12}\frac{1}{c_0}\left[\left(29-7\frac{c_1}{c_0}\right)\varepsilon_0+\left(33-13\frac{c_1}{c_0}\right)\varepsilon_1\right]+y_0+4\Delta l\tan\theta_0
\end{aligned}
\tag{A22}
$$

Observing the indicial behavior in equations (A16), (A18), (A20), and (A22), one can write the generalized first-order deflection equation for any index, $i\,(=1,\ 2,\ 3,\ldots,\ n)$, in final summation form as

$$
\begin{aligned}
y_i = {} & \frac{(\Delta l)^2}{12}\sum_{j=1}^{i}\frac{1}{c_{i-j}}\left\{\left[5+8(j-1)-\left\langle 1+2(j-1)\right\rangle\frac{c_{i-j+1}}{c_{i-j}}\right]\varepsilon_{i-j}\right. \\
& \left.+\left[3+10(j-1)-\left\langle 1+4(j-1)\right\rangle\frac{c_{i-j+1}}{c_{i-j}}\right]\varepsilon_{i-j+1}\right\}+\underbrace{y_0+(i)\Delta l\tan\theta_0}_{=0\text{ for cantilever beams}} \\
& (i=1,\ 2,\ 3,\ \ldots,\ n)
\end{aligned}
\tag{A23}
$$

which is equation (23) in the main section of this report (called the first-order displacement transfer function).

For the uniform beam ($c_i = c_{i-1} = c$), equation (A23) degenerates into

$$y_i = \frac{(\Delta l)^2}{12c} \sum_{j=1}^{i} \left\{ \left[5 + 8(j-1) - \left\langle 1 + 2(j-1) \right\rangle \right] \varepsilon_{i-j} + \left[3 + 10(j-1) - \left\langle 1 + 4(j-1) \right\rangle \right] \varepsilon_{i-j+1} \right\} + \underbrace{y_0 + (i)\Delta l \tan\theta_0}_{=0 \text{ for cantilever beams}} \qquad (i = 1,\ 2,\ 3,\ ...,\ n) \tag{A24}$$

After the terms are grouped, the deflection equation (A24) for the uniform beam takes on the form

$$y_i = \frac{(\Delta l)^2}{6c} \sum_{j=1}^{i} \left[(3j-1)\varepsilon_{i-j} + (3j-2)\varepsilon_{i-j+1} \right] + \underbrace{y_0 + (i)\Delta l \tan\theta_0}_{=0 \text{ for cantilever beams}} \qquad (i = 1,\ 2,\ 3,\ ...,\ n) \tag{A25}$$

which agrees with equation (27) of reference 2.

One can write out equation (A25) for typical indices, i (= 1, 2, 3, 4, …, n), as follows:

For i = 1,

$$y_1 = \frac{(\Delta l)^2}{6c}(2\varepsilon_0 + \varepsilon_1) + y_0 + \Delta l \tan\theta_0 \tag{A26}$$

For i = 2,

$$\begin{aligned} y_2 &= \frac{(\Delta l)^2}{6c}(2\varepsilon_1 + \varepsilon_2 + 5\varepsilon_0 + 4\varepsilon_1) + y_0 + 2\Delta l \tan\theta_0 \\ &= \frac{(\Delta l)^2}{6c}(5\varepsilon_0 + 6\varepsilon_1 + \varepsilon_2) + y_0 + 2\Delta l \tan\theta_0 \end{aligned} \tag{A27}$$

For i = 3,

$$\begin{aligned} y_3 &= \frac{(\Delta l)^2}{6c}(2\varepsilon_2 + \varepsilon_3 + 5\varepsilon_1 + 4\varepsilon_2 + 8\varepsilon_0 + 7\varepsilon_1) + y_0 + 3\Delta l \tan\theta_0 \\ &= \frac{(\Delta l)^2}{6c}\left[8\varepsilon_0 + 6(2\varepsilon_1 + \varepsilon_2) + \varepsilon_3 \right] + y_0 + 3\Delta l \tan\theta_0 \end{aligned} \tag{A28}$$

For $i = 4$,

$$\begin{aligned} y_4 &= \frac{(\Delta l)^2}{6c}(2\varepsilon_3 + \varepsilon_4 + 5\varepsilon_2 + 4\varepsilon_3 + 8\varepsilon_1 + 7\varepsilon_2 + 11\varepsilon_0 + 10\varepsilon_1) + y_0 + 4\Delta l \tan\theta_0 \\ &= \frac{(\Delta l)^2}{6c}\left[11\varepsilon_0 + 6(3\varepsilon_1 + 2\varepsilon_2 + \varepsilon_3) + \varepsilon_4\right] + y_0 + 4\Delta l \tan\theta_0 \end{aligned} \tag{A29}$$

Observing the functional behavior of equations (A26)–(A29) with an increasing index, i, one can write the generalized deflection equation for any index, $i(= 1,\ 2,\ 3,\ ...,\ n)$, for the uniform cantilever beam as

$$y_i = \frac{(\Delta l)^2}{6c}\left[(3i-1)\varepsilon_0 + 6\sum_{j=1}^{i-1}(i-j)\varepsilon_j + \varepsilon_i\right] + \underbrace{y_0 + (i)\Delta l \tan\theta_0}_{=0 \text{ for cantilever beams}} \quad ;\ (i = 1,\ 2,\ 3,\ ...,\ n) \tag{A30}$$

which agrees with equation (28) of reference 2.

APPENDIX B

DERIVATIONS OF THE SECOND-ORDER SLOPE AND DEFLECTION EQUATIONS

Appendix B presents the detailed mathematical derivations of the second-order slope equations and second-order deflection equations for the nonuniform cantilever beam.

Second-Order Slope Equations

Expanding the factor, $\left[1-\left(1-\frac{c_i}{c_{i-1}}\right)\frac{x-x_{i-1}}{\Delta l}\right]^{-1}$, in the integrand of equation (A4) in binomial series form up to the second-order term results in

$$\tan\theta(x)=\frac{\varepsilon_{i-1}}{c_{i-1}}\int_{x_{i-1}}^{x}\left[1-\left(1-\frac{\varepsilon_i}{\varepsilon_{i-1}}\right)\frac{x-x_{i-1}}{\Delta l}\right]\left[1+\left(1-\frac{c_i}{c_{i-1}}\right)\frac{x-x_{i-1}}{\Delta l}+\left(1-\frac{c_i}{c_{i-1}}\right)^2\frac{(x-x_{i-1})^2}{(\Delta l)^2}....\right]dx+\tan\theta_{i-1}$$

$$=\frac{\varepsilon_{i-1}}{c_{i-1}}\int_{x_{i-1}}^{x}\left[1+\left(1-\frac{c_i}{c_{i-1}}\right)\frac{x-x_{i-1}}{\Delta l}+\left(1-\frac{c_i}{c_{i-1}}\right)^2\frac{(x-x_{i-1})^2}{(\Delta l)^2}\right.$$

$$\left.-\left(1-\frac{\varepsilon_i}{\varepsilon_{i-1}}\right)\frac{x-x_{i-1}}{\Delta l}-\left(1-\frac{c_i}{c_{i-1}}\right)\left(1-\frac{\varepsilon_i}{\varepsilon_{i-1}}\right)\frac{(x-x_{i-1})^2}{(\Delta l)^2}-\left(1-\frac{c_i}{c_{i-1}}\right)^2\left(1-\frac{\varepsilon_i}{\varepsilon_{i-1}}\right)\frac{(x-x_{i-1})^3}{(\Delta l)^3}....\right]dx+\tan\theta_{i-1}$$

$$=\frac{\varepsilon_{i-1}}{c_{i-1}}\int_{x_{i-1}}^{x}\left[1+\left(\frac{\varepsilon_i}{\varepsilon_{i-1}}-\frac{c_i}{c_{i-1}}\right)\frac{x-x_{i-1}}{\Delta l}+\left(1-\frac{c_i}{c_{i-1}}\right)\left(\frac{\varepsilon_i}{\varepsilon_{i-1}}-\frac{c_i}{c_{i-1}}\right)\frac{(x-x_{i-1})^2}{(\Delta l)^2}\right.$$

$$\left.-\left(1-\frac{c_i}{c_{i-1}}\right)^2\left(1-\frac{\varepsilon_i}{\varepsilon_{i-1}}\right)\frac{(x-x_{i-1})^3}{(\Delta l)^3}....\right]dx+\tan\theta_{i-1}$$

$$(x_{i-1}\le x\le x_i) \quad \text{(B1)}$$

Integration of equation (B1) results in

$$\tan\theta(x)=\frac{\varepsilon_{i-1}}{c_{i-1}}\left[(x-x_{i-1})+\left(\frac{\varepsilon_i}{\varepsilon_{i-1}}-\frac{c_i}{c_{i-1}}\right)\frac{(x-x_{i-1})^2}{2\Delta l}+\left(1-\frac{c_i}{c_{i-1}}\right)\left(\frac{\varepsilon_i}{\varepsilon_{i-1}}-\frac{c_i}{c_{i-1}}\right)\frac{(x-x_{i-1})^3}{3(\Delta l)^2}\right.$$

$$\left.-\left(1-\frac{c_i}{c_{i-1}}\right)^2\left(1-\frac{\varepsilon_i}{\varepsilon_{i-1}}\right)\frac{(x-x_{i-1})^4}{4(\Delta l)^3}\right]+\tan\theta_{i-1}$$

$$(x_{i-1}\le x\le x_i) \quad \text{(B2)}$$

which is the general second-order slope equation for the domain, $x_{i-1}\le x\le x_i$.

At the strain station, $x = x_i$, we have $(x_i - x_{i-1}) = \Delta l$, and equation (B2) becomes

$$\tan\theta_i = \tan\theta(x_i) = \Delta l \frac{\varepsilon_{i-1}}{c_{i-1}} \left\{ 1 + \left(\frac{\varepsilon_i}{\varepsilon_{i-1}} - \frac{c_i}{c_{i-1}} \right) \left[\frac{1}{2} + \frac{1}{3} \left(1 - \frac{c_i}{c_{i-1}} \right) \right] - \frac{1}{4} \left(1 - \frac{c_i}{c_{i-1}} \right)^2 \left(1 - \frac{\varepsilon_i}{\varepsilon_{i-1}} \right) \right\} + \tan\theta_{i-1}$$

$$= \Delta l \frac{\varepsilon_{i-1}}{c_{i-1}} \left\{ 1 + \frac{1}{6} \left(\frac{\varepsilon_i}{\varepsilon_{i-1}} - \frac{c_i}{c_{i-1}} \right) \left(5 - 2\frac{c_i}{c_{i-1}} \right) - \frac{1}{4} \left[1 - \frac{\varepsilon_i}{\varepsilon_{i-1}} - 2\frac{c_i}{c_{i-1}} + 2\frac{c_i}{c_{i-1}}\frac{\varepsilon_i}{\varepsilon_{i-1}} + \left(\frac{c_i}{c_{i-1}} \right)^2 - \frac{\varepsilon_i}{\varepsilon_{i-1}} \left(\frac{c_i}{c_{i-1}} \right)^2 \right] \right\} + \tan\theta_{i-1}$$

$$= \frac{\Delta l}{12} \frac{\varepsilon_{i-1}}{c_{i-1}} \left\{ 12 + 10\frac{\varepsilon_i}{\varepsilon_{i-1}} - 10\frac{c_i}{c_{i-1}} - 4\frac{c_i}{c_{i-1}}\frac{\varepsilon_i}{\varepsilon_{i-1}} + 4\left(\frac{c_i}{c_{i-1}} \right)^2 - 3 + 3\frac{\varepsilon_i}{\varepsilon_{i-1}} + 6\frac{c_i}{c_{i-1}} - 6\frac{c_i}{c_{i-1}}\frac{\varepsilon_i}{\varepsilon_{i-1}} - 3\left(\frac{c_i}{c_{i-1}} \right)^2 + 3\frac{\varepsilon_i}{\varepsilon_{i-1}} \left(\frac{c_i}{c_{i-1}} \right)^2 \right\} + \tan\theta_{i-1}$$

$$(i = 1,\ 2,\ 3,\ ...,\ n) \qquad \text{(B3)}$$

After the terms are grouped, equation (B3) becomes

$$\tan\theta_i = \frac{\Delta l}{12 c_{i-1}} \left\{ \left[9 - 4\frac{c_i}{c_{i-1}} + \left(\frac{c_i}{c_{i-1}} \right)^2 \right] \varepsilon_{i-1} + \left[13 - 10\frac{c_i}{c_{i-1}} + 3\left(\frac{c_i}{c_{i-1}} \right)^2 \right] \varepsilon_i \right\} + \tan\theta_{i-1}$$

$$(i = 1,\ 2,\ 3,\ ...,\ n) \qquad \text{(B4)}$$

which is equation (28) in the main section of this report, the second-order slope equation in descending recursion form. Applying the descending recursion relationships, one can write equation (B4) in summation form as

$$\tan\theta_i = \frac{\Delta l}{12} \sum_{j=1}^{i} \frac{1}{c_{j-1}} \left\{ \left[9 - 4\frac{c_j}{c_{j-1}} + \left(\frac{c_j}{c_{j-1}} \right)^2 \right] \varepsilon_{j-1} + \left[13 - 10\frac{c_j}{c_{j-1}} + 3\left(\frac{c_j}{c_{j-1}} \right)^2 \right] \varepsilon_j \right\} + \underbrace{\tan\theta_0}_{\substack{=0 \text{ for canti-} \\ \text{lever beams}}}$$

$$(i = 1,\ 2,\ 3,\ ...,\ n) \qquad \text{(B5)}$$

which is the second-order slope equation in series summation form.

For the uniform beam, $c_i = c_{i-1} = c$, equation (B5) degenerates into

$$\tan\theta_i = \frac{\Delta l}{2c}\sum_{j=1}^{i}(\varepsilon_{j-1}+\varepsilon_j) + \underbrace{\tan\theta_0}_{\substack{=0 \text{ for canti-}\\ \text{lever beams}}} \quad ; \quad (i = 1,\ 2,\ 3,\ ...,\ n) \tag{B6}$$

which is identical to equation (25) of reference 2.

Second-Order Deflection Equations

The second-order deflection equation is obtained by carrying out the integration of the second-order slope equation (B2) as

$$\begin{aligned} y(x) &= \int_{x_{i-1}}^{x} \underbrace{\tan\theta(x)}_{\text{Eq. (B2)}}dx + y_{i-1} \\ &= \frac{\varepsilon_{i-1}}{c_{i-1}}\int_{x_{i-1}}^{x}\left[(x-x_{i-1}) + \left(\frac{\varepsilon_i}{\varepsilon_{i-1}} - \frac{c_i}{c_{i-1}}\right)\frac{(x-x_{i-1})^2}{2\Delta l} + \left(1-\frac{c_i}{c_{i-1}}\right)\left(\frac{\varepsilon_i}{\varepsilon_{i-1}} - \frac{c_i}{c_{i-1}}\right)\frac{(x-x_{i-1})^3}{3(\Delta l)^2}\right. \\ &\qquad \left. -\left(1-\frac{c_i}{c_{i-1}}\right)^2\left(1-\frac{\varepsilon_i}{\varepsilon_{i-1}}\right)\frac{(x-x_{i-1})^4}{4(\Delta l)^3}\right]dx + y_{i-1} + \int_{x_{i-1}}^{x}\tan\theta_i dx \end{aligned}$$

$$(x_{i-1} \le x \le x_i) \tag{B7}$$

After integration of equation (B7), one obtains

$$\begin{aligned} y(x) &= \frac{\varepsilon_{i-1}}{2c_{i-1}}\left[(x-x_{i-1})^2 + \frac{1}{3}\left(\frac{\varepsilon_i}{\varepsilon_{i-1}} - \frac{c_i}{c_{i-1}}\right)\frac{(x-x_{i-1})^3}{\Delta l} + \frac{1}{6}\left(1-\frac{c_i}{c_{i-1}}\right)\left(\frac{\varepsilon_i}{\varepsilon_{i-1}} - \frac{c_i}{c_{i-1}}\right)\frac{(x-x_{i-1})^4}{(\Delta l)^2}\right. \\ &\qquad \left. -\frac{1}{10}\left(1-\frac{c_i}{c_{i-1}}\right)^2\left(1-\frac{\varepsilon_i}{\varepsilon_{i-1}}\right)\frac{(x-x_{i-1})^5}{(\Delta l)^3}\right] + y_{i-1} + (x-x_{i-1})\tan\theta_{i-1} \end{aligned}$$

$$(x_{i-1} \le x \le x_i) \tag{B8}$$

which is the general second-order deflection equation for the domain, $x_{i-1} \le x \le x_i$.

At the strain station, $x = x_i$, we have $(x_i - x_{i-1}) = \Delta l$, and (B8) becomes

$$y_i \equiv y(x_i) = \frac{(\Delta l)^2}{60}\frac{\varepsilon_{i-1}}{c_{i-1}}\left[30 + 10\left(\frac{\varepsilon_i}{\varepsilon_{i-1}} - \frac{c_i}{c_{i-1}}\right) + 5\left(1 - \frac{c_i}{c_{i-1}}\right)\left(\frac{\varepsilon_i}{\varepsilon_{i-1}} - \frac{c_i}{c_{i-1}}\right) - 3\left(1 - \frac{c_i}{c_{i-1}}\right)^2\left(1 - \frac{\varepsilon_i}{\varepsilon_{i-1}}\right)\right] + y_{i-1} + \Delta l \tan\theta_{i-1}$$

$$= \frac{(\Delta l)^2}{60}\frac{\varepsilon_{i-1}}{c_{i-1}}\left\{30 + 10\frac{\varepsilon_i}{\varepsilon_{i-1}} - 10\frac{c_i}{c_{i-1}} + 5\frac{\varepsilon_i}{\varepsilon_{i-1}} - 5\frac{c_i}{c_{i-1}} - 5\frac{c_i}{c_{i-1}}\frac{\varepsilon_i}{\varepsilon_{i-1}} + 5\left(\frac{c_i}{c_{i-1}}\right)^2 - 3 + 6\frac{c_i}{c_{i-1}} - 3\left(\frac{c_i}{c_{i-1}}\right)^2 + \left[3 - 6\frac{c_i}{c_{i-1}} + 3\left(\frac{c_i}{c_{i-1}}\right)^2\right]\left(\frac{\varepsilon_i}{\varepsilon_{i-1}}\right)\right\} + y_{i-1} + \Delta l \tan\theta_{i-1}$$

$$(i = 1,\ 2,\ 3,\ ...,\ n) \qquad \text{(B9)}$$

After the terms are grouped, equation (B9) becomes

$$y_i = \frac{(\Delta l)^2}{60 c_{i-1}}\left\{\left[27 - 9\frac{c_i}{c_{i-1}} + 2\left(\frac{c_i}{c_{i-1}}\right)^2\right]\varepsilon_{i-1} + \left[18 - 11\frac{c_i}{c_{i-1}} + 3\left(\frac{c_i}{c_{i-1}}\right)^2\right]\varepsilon_i\right\} + y_{i-1} + \Delta l \tan\theta_{i-1}$$

$$(i = 1,\ 2,\ 3,\ ...,\ n) \qquad \text{(B10)}$$

which is equation (32) in the main section of this report, the second-order deflection equation in descending recursion form.

For the uniform beam, $c_i = c_{i-1} = c$, equation (B10) degenerates into

$$y_i = \frac{(\Delta l)^2}{6c}\left(2\varepsilon_{i-1} + \varepsilon_i\right) + y_{i-1} + \Delta l \tan\theta_{i-1} \quad ; \quad (i = 1,\ 2,\ 3,\ ...,\ n) \qquad \text{(B11)}$$

which agrees with equation (26) of reference 2.

Final Form of Equation (B10)

Substituting the slope equation (B5) into the deflection equation (B10), and applying the descending indicial recursion relationships, one can write out the deflection equation (B10) explicitly for each index, $i\,(= 1,\ 2,\ 3,\ ...,\ n)$, as follows:

For $i = 1$,

$$y_1 = \frac{(\Delta l)^2}{60c_0}\left\{\left[27 - 9\frac{c_i}{c_0} + 2\left(\frac{c_i}{c_{i-1}}\right)^2\right]\varepsilon_0 + \left[18 - 11\frac{c_1}{c_0} + 3\left(\frac{c_1}{c_0}\right)^2\right]\varepsilon_1\right\} + y_0 + \Delta l \tan\theta_0 \tag{B12}$$

For $i = 2$,

$$\begin{aligned} y_2 = {} & \frac{(\Delta l)^2}{60c_1}\left\{\left[27 - 9\frac{c_2}{c_1} + 2\left(\frac{c_2}{c_1}\right)^2\right]\varepsilon_1 + \left[18 - 11\frac{c_2}{c_1} + 3\left(\frac{c_2}{c_1}\right)^2\right]\varepsilon_2\right\} \\ & \underbrace{\frac{(\Delta l)^2}{60c_0}\left\{\left[27 - 9\frac{c_1}{c_0} + 2\left(\frac{c_1}{c_0}\right)^2\right]\varepsilon_0 + \left[18 - 11\frac{c_1}{c_0} + 3\left(\frac{c_1}{c_0}\right)^2\right]\varepsilon_1\right\} + y_0 + \Delta l \tan\theta_0}_{y_1} \\ & \underbrace{\frac{(\Delta l)^2}{12c_0}\left\{\left[9 - 4\frac{c_1}{c_0} + \left(\frac{c_1}{c_0}\right)^2\right]\varepsilon_0 + \left[13 - 10\frac{c_1}{c_0} + 3\left(\frac{c_1}{c_0}\right)^2\right]\varepsilon_1\right\} + \Delta l \tan\theta_0}_{\Delta l \tan\theta_1} \end{aligned} \tag{B13}$$

After the terms are grouped, equation (B13) can be written as follows:

$$\begin{aligned} y_2 = {} & \frac{(\Delta l)^2}{60c_1}\left\{\left[27 - 9\frac{c_2}{c_1} + 2\left(\frac{c_2}{c_1}\right)^2\right]\varepsilon_1 + \left[18 - 11\frac{c_2}{c_1} + 3\left(\frac{c_2}{c_1}\right)^2\right]\varepsilon_2\right\} \\ & + \frac{(\Delta l)^2}{60c_0}\left\{\left[72 - 29\frac{c_1}{c_0} + 7\left(\frac{c_1}{c_0}\right)^2\right]\varepsilon_0 + \left[83 - 61\frac{c_1}{c_0} + 18\left(\frac{c_1}{c_0}\right)^2\right]\varepsilon_1\right\} + y_0 + 2\Delta l \tan\theta_0 \end{aligned} \tag{B14}$$

For $i = 3$,

$$
\begin{aligned}
y_3 = {} & \frac{(\Delta l)^2}{60c_2}\left\{\left[27-9\frac{c_3}{c_2}+2\left(\frac{c_3}{c_2}\right)^2\right]\varepsilon_2+\left[18-11\frac{c_3}{c_2}+3\left(\frac{c_3}{c_2}\right)^2\right]\varepsilon_3\right\} \\
& \underbrace{\left\{\begin{array}{l}\dfrac{(\Delta l)^2}{60c_1}\left\{\left[27-9\dfrac{c_2}{c_1}+2\left(\dfrac{c_2}{c_1}\right)^2\right]\varepsilon_1+\left[18-11\dfrac{c_2}{c_1}+3\left(\dfrac{c_2}{c_1}\right)^2\right]\varepsilon_2\right\} \\ \quad +\dfrac{(\Delta l)^2}{60c_0}\left\{\left[72-29\dfrac{c_1}{c_0}+7\left(\dfrac{c_1}{c_0}\right)^2\right]\varepsilon_0+\left[83-61\dfrac{c_1}{c_0}+18\left(\dfrac{c_1}{c_0}\right)^2\right]\varepsilon_1\right\}+y_0+2\Delta l\tan\theta_0\end{array}\right\}}_{y_2} \\
& \underbrace{\left\{\begin{array}{l}\dfrac{(\Delta l)^2}{12c_1}\left\{\left[9-4\dfrac{c_2}{c_1}+\left(\dfrac{c_2}{c_1}\right)^2\right]\varepsilon_1+\left[13-10\dfrac{c_2}{c_1}+3\left(\dfrac{c_2}{c_1}\right)^2\right]\varepsilon_2\right\} \\ \quad +\dfrac{(\Delta l)^2}{12c_0}\left\{\left[9-4\dfrac{c_1}{c_0}+\left(\dfrac{c_1}{c_0}\right)^2\right]\varepsilon_0+\left[13-10\dfrac{c_1}{c_0}+3\left(\dfrac{c_1}{c_0}\right)^2\right]\varepsilon_1\right\}+\Delta l\tan\theta_0\end{array}\right\}}_{\Delta l\tan\theta_2}
\end{aligned}
\tag{B15}
$$

After the terms are grouped, equation (B15) can be written as follows:

$$
\begin{aligned}
y_3 = {} & \frac{(\Delta l)^2}{60c_2}\left\{\left[27-9\frac{c_3}{c_2}+2\left(\frac{c_3}{c_2}\right)^2\right]\varepsilon_2+\left[18-11\frac{c_3}{c_2}+3\left(\frac{c_3}{c_2}\right)^2\right]\varepsilon_3\right\} \\
& +\frac{(\Delta l)^2}{60c_1}\left\{\left[72-29\frac{c_2}{c_1}+7\left(\frac{c_2}{c_1}\right)^2\right]\varepsilon_1+\left[83-61\frac{c_2}{c_1}+18\left(\frac{c_2}{c_1}\right)^2\right]\varepsilon_2\right\} \\
& +\frac{(\Delta l)^2}{60c_0}\left\{\left[117-49\frac{c_1}{c_0}+12\left(\frac{c_1}{c_0}\right)^2\right]\varepsilon_0+\left[148-111\frac{c_1}{c_0}+33\left(\frac{c_1}{c_0}\right)^2\right]\varepsilon_1\right\}+y_0+3\Delta l\tan\theta_0
\end{aligned}
\tag{B16}
$$

For $i = 4$,

$$
\begin{aligned}
y_4 = {} & \frac{(\Delta l)^2}{60c_3}\left\{\left[27-9\frac{c_4}{c_3}+2\left(\frac{c_4}{c_3}\right)^2\right]\varepsilon_3+\left[18-11\frac{c_4}{c_3}+3\left(\frac{c_4}{c_3}\right)^2\right]\varepsilon_4\right\} \\
& + \underbrace{\left\{\begin{array}{l}
\dfrac{(\Delta l)^2}{60c_2}\left\{\left[27-9\dfrac{c_3}{c_2}+2\left(\dfrac{c_3}{c_2}\right)^2\right]\varepsilon_2+\left[18-11\dfrac{c_3}{c_2}+3\left(\dfrac{c_3}{c_2}\right)^2\right]\varepsilon_3\right\} \\
\quad +\dfrac{(\Delta l)^2}{60c_1}\left\{\left[72-29\dfrac{c_2}{c_1}+7\left(\dfrac{c_2}{c_1}\right)^2\right]\varepsilon_1+\left[83-61\dfrac{c_2}{c_1}+18\left(\dfrac{c_2}{c_1}\right)^2\right]\varepsilon_2\right\} \\
+\dfrac{(\Delta l)^2}{60c_0}\left\{\left[117-49\dfrac{c_1}{c_0}+12\left(\dfrac{c_1}{c_0}\right)^2\right]\varepsilon_0+\left[148-111\dfrac{c_1}{c_0}+33\left(\dfrac{c_1}{c_0}\right)^2\right]\varepsilon_1\right\}+y_0+3\Delta l\tan\theta_0
\end{array}\right\}}_{y_3} \\
& + \underbrace{\left\{\begin{array}{l}
\dfrac{(\Delta l)^2}{12c_2}\left\{\left[9-4\dfrac{c_3}{c_2}+\left(\dfrac{c_3}{c_2}\right)^2\right]\varepsilon_2+\left[13-10\dfrac{c_3}{c_2}+3\left(\dfrac{c_3}{c_2}\right)^2\right]\varepsilon_3\right\} \\
\quad +\dfrac{(\Delta l)^2}{12c_1}\left\{\left[9-4\dfrac{c_2}{c_1}+\left(\dfrac{c_2}{c_1}\right)^2\right]\varepsilon_1+\left[13-10\dfrac{c_2}{c_1}+3\left(\dfrac{c_2}{c_1}\right)^2\right]\varepsilon_2\right\} \\
+\dfrac{(\Delta l)^2}{12c_0}\left\{\left[9-4\dfrac{c_1}{c_0}+\left(\dfrac{c_1}{c_0}\right)^2\right]\varepsilon_0+\left[13-10\dfrac{c_1}{c_0}+3\left(\dfrac{c_1}{c_0}\right)^2\right]\varepsilon_1\right\}+\Delta l\tan\theta_0
\end{array}\right\}}_{\Delta l\tan\theta_3}
\end{aligned}
\tag{B17}
$$

After the terms are grouped, equation (B17) becomes

$$
\begin{aligned}
y_4 = {} & \frac{(\Delta l)^2}{60c_3}\left\{\left[27-9\frac{c_4}{c_3}+2\left(\frac{c_4}{c_3}\right)^2\right]\varepsilon_3+\left[18-11\frac{c_4}{c_3}+3\left(\frac{c_4}{c_3}\right)^2\right]\varepsilon_4\right\} \\
& +\frac{(\Delta l)^2}{60c_2}\left\{\left[72-29\frac{c_3}{c_2}+7\left(\frac{c_3}{c_2}\right)^2\right]\varepsilon_2+\left[83-61\frac{c_3}{c_2}+18\left(\frac{c_3}{c_2}\right)^2\right]\varepsilon_3\right\} \\
& +\frac{(\Delta l)^2}{60c_1}\left\{\left[117-49\frac{c_2}{c_1}+12\left(\frac{c_2}{c_1}\right)^2\right]\varepsilon_1+\left[148-111\frac{c_2}{c_1}+33\left(\frac{c_2}{c_1}\right)^2\right]\varepsilon_2\right\} \\
& +\frac{(\Delta l)^2}{60c_0}\left\{\left[162-69\frac{c_1}{c_0}+17\left(\frac{c_1}{c_0}\right)^2\right]\varepsilon_0+\left[213-161\frac{c_1}{c_0}+48\left(\frac{c_1}{c_0}\right)^2\right]\varepsilon_1\right\}+y_0+4\Delta l\tan\theta_0
\end{aligned}
\tag{B18}
$$

Observing the indicial progressions in equations (B12), (B14), (B16), and (B18), one can write the generalized second-order deflection equation for any index, $i(=1,\ 2,\ 3,\ ...,\ n)$, in series summation form as

$$
\begin{aligned}
y_i = {} & \frac{(\Delta l)^2}{60}\sum_{j=1}^{i}\frac{1}{c_{i-j}}\left\{\left[27+45(j-1)-\left\langle 9+20(j-1)\right\rangle\frac{c_{i-j+1}}{c_{i-j}}+\left\langle 2+5(j-1)\right\rangle\left(\frac{c_{i-j+1}}{c_{i-j}}\right)^2\right]\varepsilon_{i-j}\right. \\
& \left.+\left[18+65(j-1)-\left\langle 11+50(j-1)\right\rangle\frac{c_{i-j+1}}{c_{i-j}}+\left\langle 3+15(j-1)\right\rangle\left(\frac{c_{i-j+1}}{c_{i-j}}\right)^2\right]\varepsilon_{i-j+1}\right\}+\underbrace{y_0+(i)\Delta l\tan\theta_0}_{=0\text{ for cantilever beams}} \\
& (i=1,\ 2,\ 3,\ ...,\ n)
\end{aligned}
\tag{B19}
$$

which is equation (34) in the main section of this report, called the second-order displacement transfer function.

For the uniform beam, $c_i = c_{i-1} = c$, equation (B19) degenerates into

$$y_i = \frac{(\Delta l)^2}{60c} \sum_{j=1}^{i} \left\{ \left[27 + 45(j-1) - \left\langle 9 + 20(j-1) \right\rangle + \left\langle 2 + 5(j-1) \right\rangle \right] \varepsilon_{i-j} \right.$$
$$\left. + \left[18 + 65(j-1) - \left\langle 11 + 50(j-1) \right\rangle + \left\langle 3 + 15(j-1) \right\rangle \right] \varepsilon_{i-j+1} \right\} + y_0 + (i)\Delta l \tan\theta_0$$
$$= \frac{(\Delta l)^2}{60c} \sum_{j=1}^{i} \left\{ \left[20 + 30(j-1) \right] \varepsilon_{i-j} + \left[10 + 30(j-1) \right] \varepsilon_{i-j+1} \right\} + y_0 + (i)\Delta l \tan\theta_0$$
$$(i = 1,\ 2,\ 3,\ ...,\ n) \qquad \text{(B20)}$$

which can be written in a compact form as

$$y_i = \frac{(\Delta l)^2}{6c} \sum_{j=1}^{i} \left[(3j-1)\varepsilon_{i-j} + (3j-2)\varepsilon_{i-j+1} \right] + \underbrace{y_0 + (i)\Delta l \tan\theta_0}_{=0 \text{ for cantilever beams}}$$
$$(i = 1,\ 2,\ 3,\ ...,\ n) \qquad \text{(B21)}$$

which is identical to equation (A25) of Appendix A.

REFERENCES

1. Ko, William L., W.L. Richards, and Van T. Tran, *Displacement Theories for In-Flight Deformed Shape Predictions of Aerospace Structures*, NASA/TP-2007-214612, 2007.

2. Ko, William L. and Van Tran Fleischer, *Further Development of Ko Displacement Theory for Deformed Shape Predictions of Nonuniform Aerospace Structures*, NASA/TP-2009-214643, 2009.

3. Ko, William L., W. Lance Richards, and Van Tran Fleischer, *Applications of Ko Displacement Theory to the Deformed Shape Predictions of the Doubly-Tapered Ikhana Wing*, NASA/TP-2009-214652, 2009.

4. Ko, William L. and Van Tran Fleischer, *Methods for In-Flight Wing Shape Predictions of Highly Flexible Unmanned Aerial Vehicles: Formulation of Ko Displacement Theory*, NASA/TP-2010-214656, 2010.

5. Ko, William L. and William Lance Richards, *Method for Real-Time Structure Shape-Sensing*, U.S. Patent No. 7,520,176, issued April 21, 2009.

6. Richards, William Lance and William L. Ko, *Process for Using Surface Strain Measurements to Obtain Operational Loads for Complex Structures*, U.S. Patent No. 7,715,994, issued May 11, 2010.

7. Bang, Hyung-Joon, Hyun-Kyu Kang, Chang-Sun Hong, and Chun-Gon Kim, "Optical Fiber Sensor Systems for Simultaneous Monitoring of Strain and Fractures in Composites," *Smart Materials and Structures*, Vol. 14, Sept. 2005, pp. N52–N58.

8. Wehrle, Günther, Percy Nohama, Hypolito José Kalinowski, Pedro Ignácio Torres, and Luiz Carlos Guedes Valente, "A Fiber Optic Bragg Grating Strain Sensor for Monitoring Ventilatory Movements," *Measurement Science and Technology*, Vol. 12, April 2001, pp. 805–809.

9. Baldwin, Christopher S., Toni J. Salter, and Jason S. Kiddy, "Static Shape Measurements Using A Multiplexed Fiber Bragg Grating Sensor System," *Proceedings of Smart Structures and Materials 2004: Smart Sensor Technology and Measurement Systems*, edited by Eric Udd and Daniele Inaudi, SPIE Vol. 5384, San Diego, March 15, 2004, pp. 206–217.

10. Ko, William L. and Van Tran Fleischer, *Extension of Ko Straight-Beam Displacement Theory to Deformed Shape Predictions of Slender Curved Structures*, NASA/TP-2011-214657, 2011.

11. Roark, Raymond J., *Formulas for Stress and Strain*, Third Edition, McGraw-Hill Book Company, Inc., New York, 1954.

12. Faupel, Joseph H., *Engineering Design: A Synthesis of Stress Analysis and Materials Engineering*, John Wiley and Sons, Inc., New York, 1964.

13. Hodgman, Charles D., *Standard Mathematical Tables*, Seventh Edition, Chemical Rubber Publishing Company, Cleveland, 1957.

14. Whetstone, W.D., *SPAR Structural Analysis System Reference Manual*, System Level 13A, Vol. 1, Program Execution, NASA CR-158970-1, 1978.